

FINAL PUBLISHABLE JRP REPORT

JRP-Contract number	EXL02	
JRP short name	SIQUTE	
JRP full title	Single-photon sources for quantum technologies	
Version numbers of latest contracted Annex Ia and Annex Ib against which the assessment will be made	Annex Ia:	V1.1
	Annex Ib:	V1.0
Period covered (dates)	From 01 June 2013	To 31 May 2016
JRP-Coordinator		
Name, title, organisation	Dr. Stefan Kück	
Tel:	+49 (0)531 592 4100	
Email:	stefan.kueck@ptb.de	
JRP website address	http://www.ptb.de/emrp/siqute-home.html	
Other JRP-Partners		
Short name, country	PTB, Germany	
	CMI, Czech Republic	
	INRIM, Italy	
	Metrosert, Estonia	
	MIKES, Finland	
	NPL, United Kingdom	
	USMF, United States	
REG-Researcher (associated Home Organisation)		
Researcher name, title (Home organisation Short name, Country)	Dr. Julien Claudon (CEA, France)	Start date: 01.06.2013 Duration: 24 months
Researcher name, title (Home organisation Short name, Country)	Dr. Niels Gregersen (DTU, Denmark)	Start date: 01.06.2013 Duration: 18 months

Report Status: PU Public



Researcher name, title
(Home organisation Short
name, Country)

Dr. Stephan Götzinger
(FAU, Germany)

Start date: 01.06.2013

Duration: 24 months

Researcher name, title
(Home organisation Short
name, Country)

Dr. Christoph Becher
(UDS, Germany)

Start date: 01.06.2013

Duration: 24 months

Researcher name, title
(Home organisation Short
name, Country)

Dr. Jesper Mork
(DTU, Denmark)

Start date: 01.11.2013

Duration: 18 months



TABLE OF CONTENTS

1 Executive Summary 4

2 Project context, rationale and objectives 5

3 Research results 5

 Development of bright, compact and near-unity collection efficiency single-photon sources with a photon flux of up to 10^7 photon/s based on quantum dots, vacancies in nanodiamonds and photonic waveguide technologies..... 5

 Characterisation of these single-photon sources by appropriate metrics in terms of wavelength, bandwidth, photon statistics, anti-bunching, and indistinguishability..... 14

 Development of an excitation scheme with adjustable frequency allowing for traceable photon flux measurements..... 17

 Demonstration of the suitability of single-photon sources for different entanglement enhanced measurements 24

 Summary of the key results and conclusions of the research undertaken 26

4 Actual and potential impact 29

 Actual and potential impact 29

 Dissemination of results 29

 Potential impact 29

5 Website address and contact details 29

6 List of publications..... 29

1 Executive Summary

Introduction

Photons are mass-less elementary particles which have the potential to be used for quantum communication, computing and metrology applications. In order to meet the scientific criteria of these applications, single photons, which will have unique characteristics, are required. This project developed compact and efficient single-photon sources, and suitable measurement techniques for the characterisation of these sources.

The Problem

Single-photon sources have a large variety of applications in the field of metrology. Furthermore, deterministic, compact and efficient single-photon sources (SPS) are required for cutting edge quantum optical technologies such as quantum communication, quantum computation, quantum metrology and quantum radiometry. Until the beginning of this project, neither single-photon-sources nor metrology-based characterization of such sources existed. This project arose from the fact that up to now no single-photon-source existed that fulfils all the requirements needed for quantum communication and computing, quantum metrology and quantum-based radiometry and there was no metrological infrastructure for single photon detectors.

The Solution

Within this project, different types of single-photon sources have been researched using different approaches, such as based on impurity centres in diamond, quantum dots or based on waveguide structures, and they have been metrologically characterised. In the participating NMIs, setups for the traceable measurement of wavelength, bandwidth, photon statistics, anti-bunching, and indistinguishability were established therefore, single photon sources are now established within the NMIs and are available for use in wider fields of metrology, i.e. quantum-based radiometry and specific fields of quantum metrology.

Impact

This project developed compact and efficient single-photon sources, and suitable measurement techniques for the characterisation of these sources.

The results achieved within the project will support the development of better and easier-to-use single-photon sources. The sub-ns pulse diode laser driving electronics with adjustable frequency for excitation of single-photon sources developed in the second objective of the project will be useful for further investigation of different types of single-photon sources, because it allows a scaling up of the photon flux by increasing the repetition rate instead of by increasing the excitation power. Antenna designs for simplification of photon collection were also developed and characterised by the project, as well as the high efficient waveguide-based single-photon source.

The results of this project have been reported in 28 peer-reviewed publications and activities have been presented in 72 talks or posters at scientific conferences. Furthermore, guidelines dealing with the calibration and the alignment of Silicon-based single-photon avalanche detectors were uploaded to the SIQUTE project website located at: www.ptb.de/emrp/siqute.html.

The output of the SIQUTE project was not to “produce” some kind of device, which will be used by any type of end user directly. This project was, amongst others, meant to bring single-photon and quantum technology more into the metrology fields of radiometry. So end users will finally be manufacturers of devices for single-photon and quantum metrology related devices, such as quantum key distribution systems, single-photon detectors, as eventually single-photon sources. Therefore, potential uptake by end users was promoted through the dissemination and standardisation activities.

2 Project context, rationale and objectives

Photons can be generated from vacancy centres within nanocrystals, in this case nitrogen vacancies in diamonds. This relies on artificially producing a diamond and irradiating it to produce a single vacancy centre. Then irradiating the vacancy with a laser pulse to cause it to emit a photon. To be useful the direction of this photon needs to be controlled, so methods of improving collection efficiency are also required.

Single photon sources can also be emitted from quantum dots, in this case indium arsenide (InAs) quantum dots within a gallium arsenide (GaAs) structure. These have the potential to emit photons by electrical excitation, which should make the process easier, but they do need very low temperatures 12-20 K.

Photon entanglement occurs when two photons have a relationship or correlation, so that knowing characteristics of one will give information about the other. This is a fragile phenomenon, which makes it difficult to measure but means that it has the potential to measure small forces and absorptions that cannot be done in any other method.

Studying photon sources have to be done in parallel with the development of detectors. Currently, no NMI can calibrate a single photon detector in a proven way. Therefore, this project aimed to set up calibration and characterisation services.

The following four objectives were identified to achieve the overall goal of developing efficient single-photon sources and their underpinning metrological infrastructure. Objective 1 dealt with the development of bright, compact and efficient single-photon sources based on quantum dots and vacancies in nanodiamonds. Objective 2 looked at controlling the excitation, and thus the production of photons, by adjusting the frequency. Objective 3 characterised the sources with appropriate metrics such as wavelength, bandwidth, photon statistics, anti-bunching and indistinguishability. Finally, in objective 4, the possibility and potential of using single-photon sources and entanglement for quantum enhanced measurements were explored.

The objectives were:

- The development of bright, compact and near-unity collection efficiency single-photon sources with a photon flux of up to 10^7 photon/s based on quantum dots, vacancies in nanodiamonds and photonic waveguide technologies;
- The development of an excitation scheme with adjustable frequency allowing for traceable photon flux measurements at high photon rate to be utilised in the calibration of very low photon rates;
- the characterisation of these single-photon sources by appropriate metrics in terms of wavelength, bandwidth, photon statistics, anti-bunching, and indistinguishability;
- The demonstration of the suitability of these sources for different entanglement-enhanced measurements based on those metrics.

3 Research results

Development of bright, compact and near-unity collection efficiency single-photon sources with a photon flux of up to 10^7 photon/s based on quantum dots, vacancies in nanodiamonds and photonic waveguide technologies

Within this project, different types of single-photon sources have been researched, i.e. single-photon sources based on defect centres in nanodiamond, based on semiconductor quantum dots and based on photonic waveguide structures.

3.1.1 Single-photon sources based on defects centres in nanodiamonds

One approach carried out was the investigation towards the realisation of single-photon sources based on impurity centres in diamond, namely nitrogen-vacancy centres (NV-centres) and silicon-vacancy centres (SiV-centres). Although impurity doped nanodiamonds as bases for single-photon sources have been known for some years now, they typically lack reproducibility in the production process as well as high efficiencies due to rather poor collection efficiency for the emitting photons. Therefore, the first goals of this project were the investigation of suitable production processes. These attempts were carried out at REG4(UDS), who produced nanodiamonds on tailored substrates via Chemical Vapour Deposition (CVD) growth. The

substrate consists of a composite structure with an Iridium layer on top and prior to the CVD growth an array of marker structures was fabricated in the Iridium-layer. On small seed diamonds microwave CVD growth is performed. The resulting nanodiamonds have sizes of about 100 nm; a reasonable number of nanodiamonds contain single silicon-vacancy-centres (SiV). By overlaying white light scans, fluorescence scans and Scanning Electron Microscope (SEM) pictures, individual nanodiamonds containing single SiV-centres were registered with the markers. This procedure was established by REG(UDS), a written report was sent to PTB. A sample containing 10 nanodiamonds with single SiV-centres, together with spectroscopy data and preliminary photon statistics measurements has been sent by REG(UDS) to PTB. NV-centres were not produced by CVD-method, because they were commercially available. Furthermore, NV- and SiV-centre nanodiamonds were also produced by bead-assisted sonic disintegration (BASD). Two approaches have been successfully investigated, i.e. (a) the implantation of Si into "microdiamonds" (milled from Element Six polycrystalline diamond) and annealing; this produced SiV-centres and further milling to nanodiamonds were carried out and (b) the milling of polycrystalline diamond (source: O. Williams, Cardiff University), which resulted in nanodiamonds of 100 nm size containing single SiV-centres. For the production of BASD diamonds containing NV-centres, two approaches have been investigated, i.e. (a) milled nanodiamonds (source: J. Stursa, Academy of Sciences of the Czech Republic), which contain a few NV-centres per nanodiamond, so that single NV-centres were not found and (b) the milling of polycrystalline diamond (Element Six), which were irradiated with electrons and finally resulted in nanodiamonds containing single NV-centres. Spectroscopic measurements of three samples of nanodiamonds of sizes of 50 nm, 70 nm and 100 nm containing SiV-centres have been performed by REG(UDS) A specific distribution of the width of the zero phonon line (ZPL) with respect to its centre wavelength were found: ZPLs, which are shifted with respect to the characteristic ZPL wavelength of 738 nm exhibit linewidths smaller than 2 nm; ZPLs at around 738 nm are broader, up to as much as 14 nm. We exemplarily calculated the Debye-Waller factor of a representative SiV-centre which is 0.81 ± 0.01 . Photon autocorrelation measurements revealed numerous emitters to be single SiV-centres, independent of the ZPL centre wavelength or the ZPL linewidth. The overall detection efficiency of the confocal setup has been measured for a particular emitter at a specific wavelength (764 nm) to be $(14 \pm 4) \%$ without collection efficiency of the microscope objective and $(0.16 \pm 0.04) \%$ including the collection efficiency for an objective with a numerical aperture NA of 0.8 and an emitter in a structured diamond film.

The nanodiamonds produced at REG(UDS) were implemented into dielectric structures at REG(FAU). First, REG(FAU) determined the design parameters for incorporating nitrogen-vacancy (NV) centres and silicon-vacancy (SiV) centres in diamond. Several potential materials were identified for use in conjunction with these single-photon sources in the metal-dielectric antenna structure, including polymers (PMMA, PVA, and CYTOP) and crystals (MgF_2). These materials are compatible both with silica-based cover glasses and sapphire cover glasses. REG(FAU) realized several metal-dielectric antennas using the above mentioned single photon sources with a cover glass as the substrate. Theoretical simulations show that these antenna designs allow for collection efficiencies higher than 99 %. REG(FAU) also suggested several designs with NV- or SiV-centres on solid immersion lenses (SIL) as substrate together with a long distance air objective ($\text{NA} = 0.8$), which can be used in cryogenic environment. A list of suitable materials was assembled by REG(FAU), containing polymers (PMMA, PVA, and CYTOP) and crystals (MgF_2). For each material, the fluorescence count rate was measured using an avalanche photodiode and under excitation with a 532 nm laser. All the materials have acceptable fluorescence count rates, in the order of 10^3 or less. CYTOP leads to an order of magnitude larger count rate compared to PMMA, PVA or MgF_2 , so was excluded from further investigations. REG(FAU) fabricated dielectric antennas with the materials and design parameters described above. The antennas contained single NV- and SiV-centres, showed low fluorescence background and showed single photon emission. The uncertainty in the flux rate was 3 %, however, this neglects the effect of quantum efficiency, which is not known for the defects in the samples. Preliminary measurements have shown that the count rates deviate from what is expected from the lifetime of the defect centres. It appears that the quantum efficiency for NV- and SiV-centres deviate significantly from 1. Another series of measurements were carried out by PTB and REG(FAU) in cooperation of REG(UDS) in order to investigate the defect centres of a new set of NV. The concern about the quantum efficiency has been confirmed by these measurements. It also seems that the quantum efficiency can vary strongly from defect to defect. The issue on the quantum efficiency of NV- and SiV-centres in nanodiamonds is not solved yet and needs to be further investigated. With the NV-centre doped nanocrystals photon rates of up to 700 kcps with a $g^2(0)$ -value as low as 0.06 for nanodiamonds on standard cover glass and photon rates up to 2.9 Mcps for nanodiamonds on an additional MgF_2 layer with a $g^2(0)$ -value of 0.34 were obtained.

One of the major outcomes of this project is the experimental realization and the absolute characterization of a NV-centre based single-photon source in terms of wavelength, background, g^2 , stability and photon flux. The single-photon source was absolutely calibrated with respect to its photon flux and its spectral photon rate density. The absolute photon flux was measured with a low noise silicon photodiode traceable to the primary standard for optical flux taking into account the absolute spectral power distribution using a calibrated spectroradiometer, see the traceability chain in Figure 1. The optical radiant flux is adjustable from 55 fW, which is almost the lower detection limit for the silicon photodiode, and 75 fW, which is the saturation power of the NV-centre. These fluxes correspond to total photon flux rates between 190 000 photons per second and 260 000 photons per second, respectively, see Figure 2. The single-photon emission purity is indicated by a $g^{(2)}(0)$ -value, which is between 0.10 and 0.23, depending on the excitation power. Also the saturation behaviour and the background emission behaviour were calculated from the measured $g^{(2)}(0)$ -values, see also Figure 2, using the equation:

$$N_{\text{ph}} = \frac{N_{\text{sat}}}{1 + \frac{P_{\text{sat}}}{P}} + mP, \quad (1)$$

where $N_{\text{sat}} = 240\,000\text{ s}^{-1}$ is the saturation photon flux, $P_{\text{sat}} = 100\ \mu\text{W}$ is the saturation power and $m = 27.6\ \mu\text{W}^{-1}\text{s}^{-1}$ is the linear power coefficient for the background fluorescence.

In Figure 3, the spectra of the NV-centre emission are shown, given in absolute photon flux per wavelength $N_{\text{ph},\lambda}(\lambda)$ and in absolute radiant flux per wavelength $\Phi_{\lambda}(\lambda)$. To our knowledge, this is the first single-photon source absolutely calibrated with respect to its absolute optical radiant flux and spectral power distribution, traceable to the corresponding national standards via an unbroken traceability chain. The prospects for its application, e.g. for the detection efficiency calibration of single-photon detectors as well as for the use as a standard photon source in the low photon flux regime, are promising. A manuscript with authors from CMI, PTB, REG(FAU) and REG(UDS) was submitted in August 2016 to a peer-reviewed journal (*B. Rodiek et al., submitted to Optica*).

Another important issue was tackled in this project, i.e. the issue of the total coupling efficiency between the emitter, i.e. the NV- or SiV-centre in nanodiamond, and the detector. The coupling efficiency measurement of the setup was carried out by using a laser source at 670 nm in three steps: First, the input optical power P_{in} is measured with a calibrated optical power meter. Second, the fibre pigtail of the laser source is connected to the setup and the optical power P_{out} after the objective is measured. Third, the insertion loss due to the connectors is separately measured by using a SM-Optical fibre from the same type that the one used in the setup. The complete evaluation of the coupling efficiency η_c gave $\eta_c = 23.8\ \% \pm 0.8\ \%$.

A predictable single-photon source (SPS) based on a silicon vacancy centre in nanodiamond was also realized, however, with less photon flux. The SPS was optically pumped with a laser at 685 nm with repetition rates between 10 MHz and 70 MHz and with pulses of approx. 50 ps length. A linear dependence of the number of emitted photons on the repetition rate was observed. Therefore, such a source can be used for the calibration of photodetectors for optical fluxes of approx. 10 000 photons/s to 60 000 photons/s, which is unreachable by conventional calibrated photodetectors. The measurement uncertainty is in the order of 1 %. For details, see also section 3.1.9.

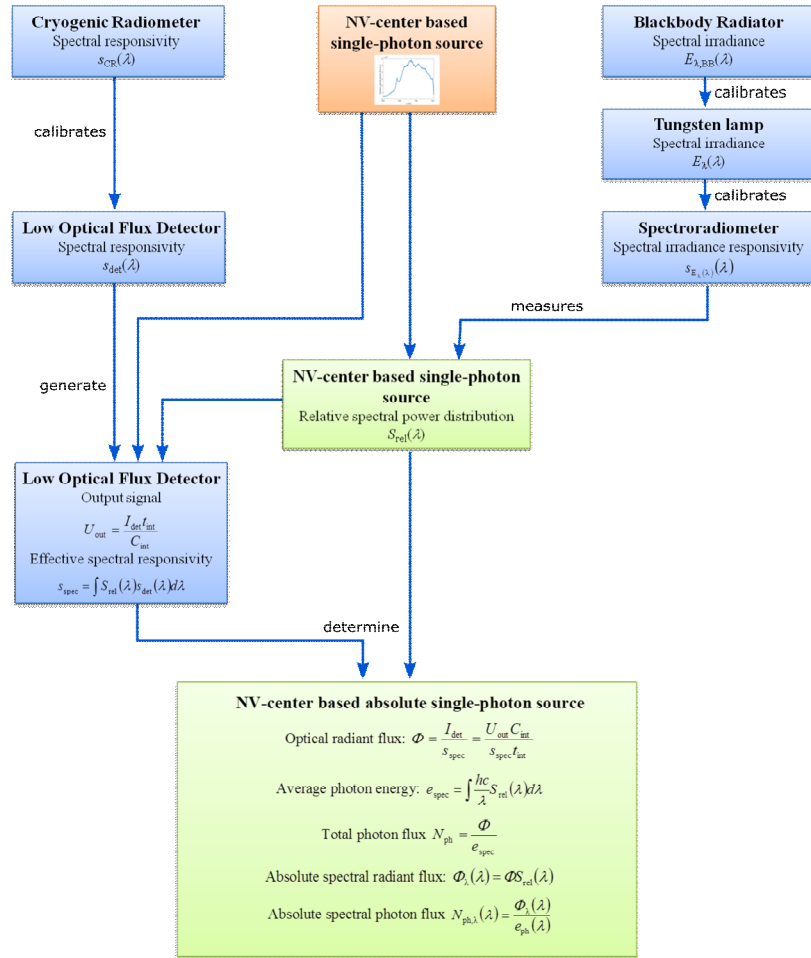


Figure 1: Schematic overview of the necessary measurements, calibrations and calculations for the characterization of the absolute NV-centre based single-photon source.

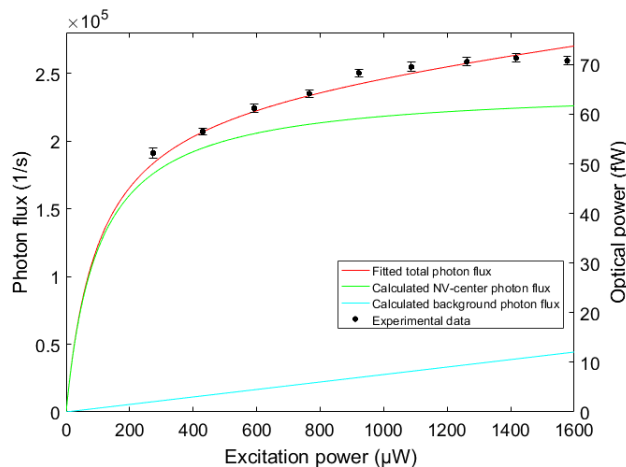


Figure 2: Left axis: The total number of photons, emitted by the NV-centre, as a function of the excitation power of a 532 nm laser, measured with the high sensitive photodiode detector build by CMI. Right axis: Corresponding total optical power. The error bars correspond to the standard uncertainty. The red, green and blue curves are the total photon flux, the NV-centre photon flux and the background photon flux, respectively, calculated from eqn. (1) using the fit parameters $N_{sat} = 240\,000\text{ s}^{-1}$, $P_{sat} = 100\ \mu W$ and $m = 27.6\ \mu W^{-1} s^{-1}$.

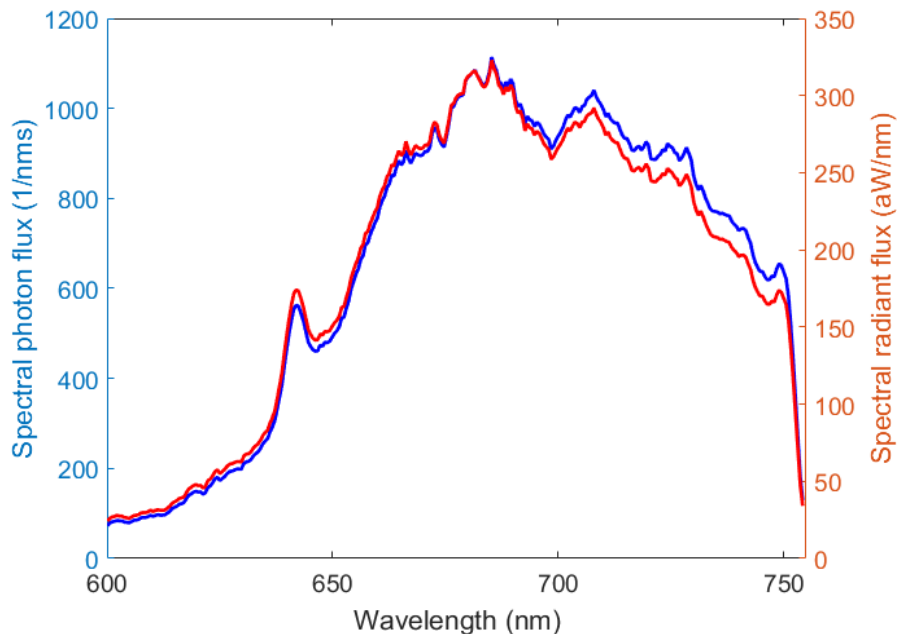


Figure 3: Spectra of the NV-centre emission given in absolute photon flux per wavelength $N_{ph,\lambda}(\lambda)$ (blue line) and in absolute radiant flux per wavelength $\Phi_{\lambda}(\lambda)$ (red line).

In addition to the activities concerning diamond defect centres in dielectric antennas, a metal-dielectric antenna was designed and realized by REG(FAU), which collected more than 99 % of the emitted photons from single colloidal quantum dots, see X.-L. Chu *et al.*, *Optica* 1, 203 (2014) [Ref. 7].

3.1.2 Single-photon sources based on quantum dots

The second approach for an efficient single-photon source was based on semiconductor quantum dots in semiconductor structures.

Within this project, designs and concepts for the single-photon sources based on semiconductor quantum dots were developed and formulated by REG(DTU). The sequence of developments within this project was first, to develop an optically pumped nanowire single-photon source, second to develop an optically pumped elliptical nanowire single-photon source designed for an efficiency > 0.85 and with polarization control and third to develop a nanowire single-photon source with electrical injection and a first lens external efficiency of 50 %, $g^2(0) < 0.1$ and a photon rate of approx. 35 MHz. These steps were addressed subsequently by modelling the appropriate design by REG(DTU), manufacturing the device by REG(CEA) and finally investigate the manufactured samples in terms of second order correlation function ($g^{(2)}(0)$ -value), spectral characteristics and photon rate by PTB.

An example of the result of the modelling is shown in Figure 4, where an optically pumped elliptical nanowire single-photon source with efficiency > 0.85 and polarization control was designed. The full vectorial elliptical mode profiles were calculated and a vectorial solver was set up. The bottom mirror reflection coefficient and the critical emitter-mirror distance for the elliptical design were identified.

The manufactured optically pumped nanowire single-photon source, in specific the design of a photonic trumpet for high mode matching, is exemplarily shown in Figure 5. The whole structure consisted of an ensemble of wires with circular and elliptical sections. These wires, which neither feature any bottom mirror nor top taper, offer an extraction efficiency in the 10 %-15 % range.

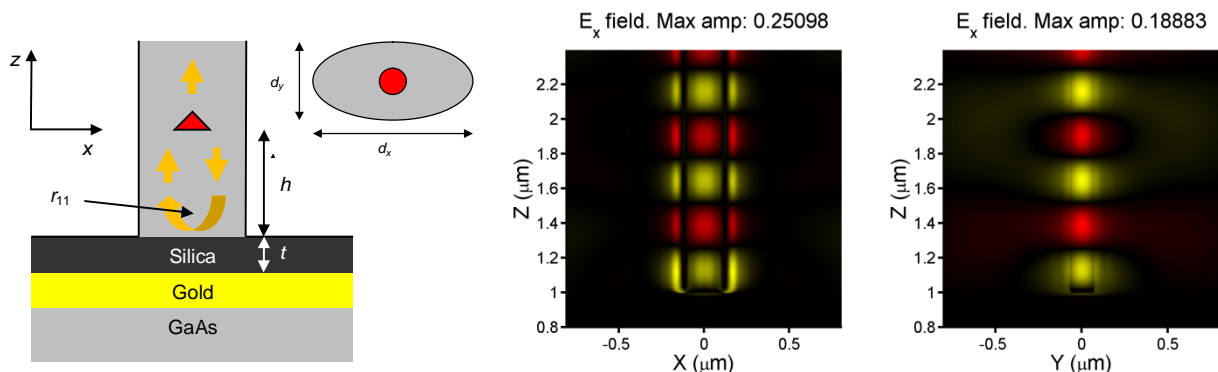


Figure 4: left: bottom part of the elliptical nanowire geometry and cross-section, middle and right: electrical field E_x component along the major (middle) and minor (right) semi-axis for the elliptical nanowire geometry.

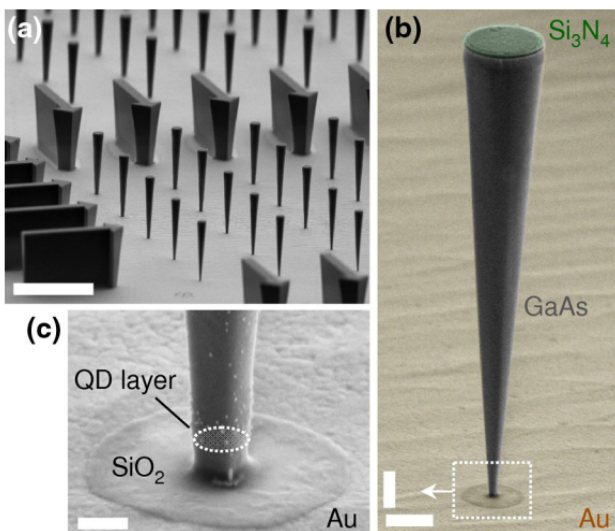


Figure 5: Single-photon trumpets. (a) Scanning electron microscope view, scale bar: 15 μm . (b) Single trumpet, scale bars: 1 μm . (c) Trumpet bottom showing the localization of the quantum dot layer and the integrated mirror, scale bar: 200 nm.

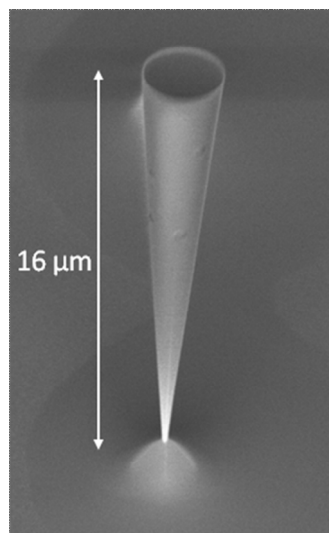


Figure 6: GaAs (Gallium Arsenide) photonic trumpet with an elliptical base which is compatible with polarization control.

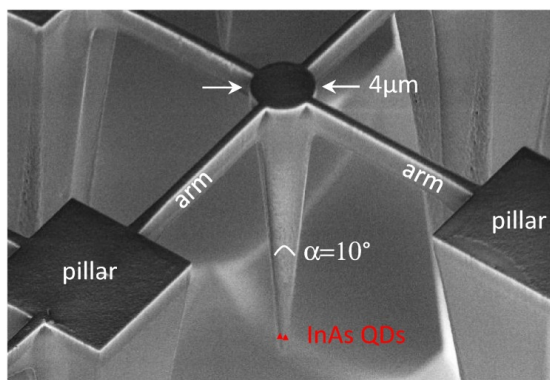


Figure 7: The suspended trumpet design.

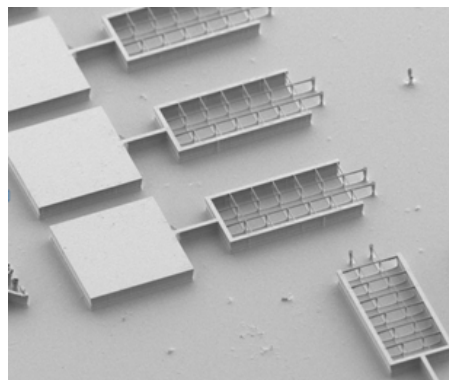


Figure 8: Nanowire single-photon source with electrical injection (first lens external efficiency 50 %, $g^2(0) < 0.1$, photon rate approx. 35 MHz delivered).

A GaAs (Gallium Arsenide) photonic trumpet with an elliptical base which is compatible with polarization control was realized. The fabrication work includes the Molecular Beam Epitaxy (MBE) growth of a sample, e-beam lithography and reactive-ion etching (RIE). Two tilted observations by SEM reveal that the base of the trumpet is compatible with single mode emission as well as with polarized emission, because the diameters are 260 nm and 150 nm. The top diameter (2.3 μm) is compatible with a directive emission, completely intercepted by a numerical aperture of 0.8. Figure 6 shows a SEM view of an elliptical trumpet-like taper. Furthermore, a new ‘suspended trumpet design’ was introduced to improve mechanical stability, see Figure 7. The photonic trumpet is suspended and anchored to four pillars with arms connected to its top facet. The fabrication work includes the MBE growth of a sample, e-beam lithography and reactive-ion etching. Isolated Indium arsenide (InAs) quantum dots are located in the base of the structure, which features an elliptical cross-section. The base dimensions (minor diameter = 150 nm and major diameter = 300 nm) are compatible with single-mode emission. The top facet diameter (around 4 μm) ensures a very directive emission, completely intercepted by a numerical aperture of 0.8. Considering the sample geometry, an extraction efficiency in the 40 % range is predicted for an on-axis emitter. Preliminary optical measurements reveal a pronounced linear far-field polarisation (degree of linear polarisation = 80 %).

All these samples were investigated and characterized with respect to the single-photon properties, i.e. the second order correlation function, the spectral characteristics and the photon rate. Unfortunately, within the frame of this project, the aimed goals could not be achieved. Single-photon emission was not observed in all these samples. The reason is that the photonic trumpets contain too many QDs, so that for an observation of single photon emission spectral filtering is required, see for illustration Figure 9. Despite efforts to perform this by using spectrometers or combinations of band pass filters, it was until the end of the project not possible to realize appropriate filtering, so that the observation of non-classical light thus far failed. For the electrical pumping, the nanowire single-photon source with electrical injection was delivered, accompanied by a detailed description, to PTB in February 2016. However, the electrical contacting failed, so that electrical excited single photon emission could not be observed within the project lifetime.

Alternatively, also another approach was carried out. A semiconductor quantum-dot-embedded microlens structure was fabricated in the Institut für Festkörperphysik at the Technical University of Berlin (Working Group Prof. Stephan Reitzenstein). The quantum dot emission was spectrally filtered to a single line at 921.5 nm, which emitted single-photon emission with a $g^{(2)}(0)$ value of 0.2 and a photon rate of approx. 240 000 photons per second. Thus, in conclusion, single photon emission of a semiconductor-based sample was finally obtained within the consortium. The spectrum, the filtered spectrum and the measurement of the 2nd order correlation function are shown in Figure 10.

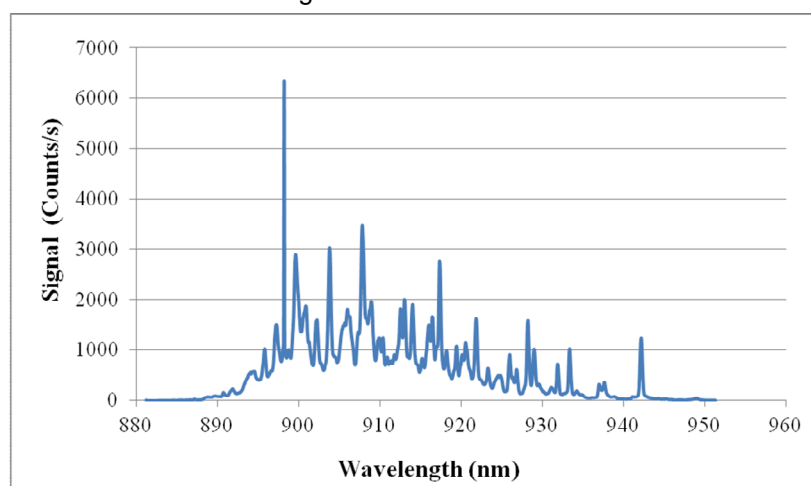


Figure 9: Photoluminescence spectrum of quantum dots contained in a single-photon photonic trumpet.

Report Status: PU Public

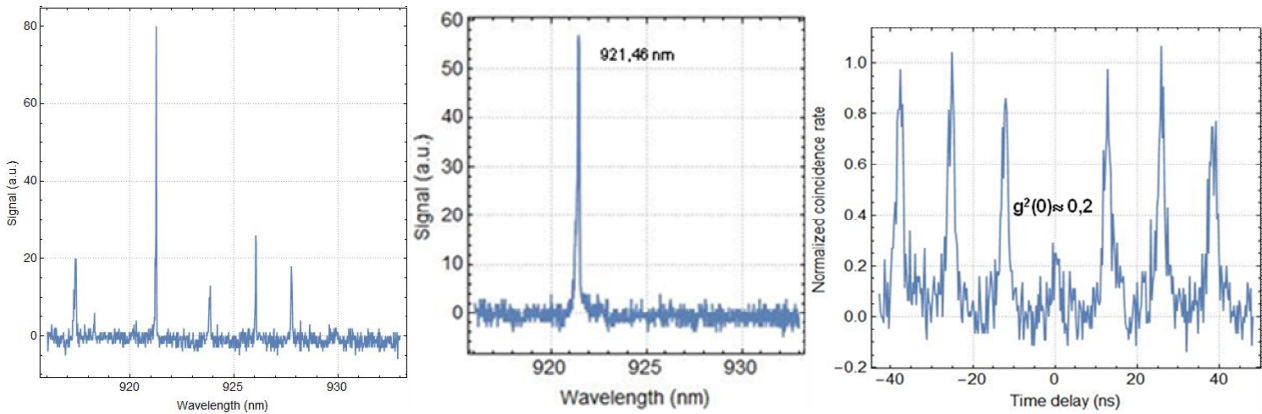


Figure 10: left) Emission spectrum of the InGaAs/GaAs QD-microlens structure, middle spectrum after spectral filtering, right) second order correlation function.

3.1.3 Single-photon sources based on waveguide structures

The third approach for efficient single-photon sources within this project was based on nonlinear processes in waveguide structures. In specific, the work aimed towards the generation of single photons in the telecom band. Thus, an experiment for the generation of single photons in the telecom band based on spontaneous parametric down-conversion (SPDC) was set-up at REG(UDS) and the data sets to be measured were specified by NPL, PTB and REG(UDS), i.e. the temporal and spectral properties of the down-converted photons; their down-conversion and heralding efficiencies; the photon statistics; the indistinguishability between separate heralded photons; and joint spectral distribution. The process employed is based on the spontaneous decay of a pump photon at 710 nm into signal and idler photons at 1310 nm and 1550 nm. A tuning range of parametric fluorescence from 1295 nm – 1350 nm and 1510 nm - 1580 nm, thus covering the full telecom O- and C-bands, were observed. The experimental setup is shown in Figure 11.

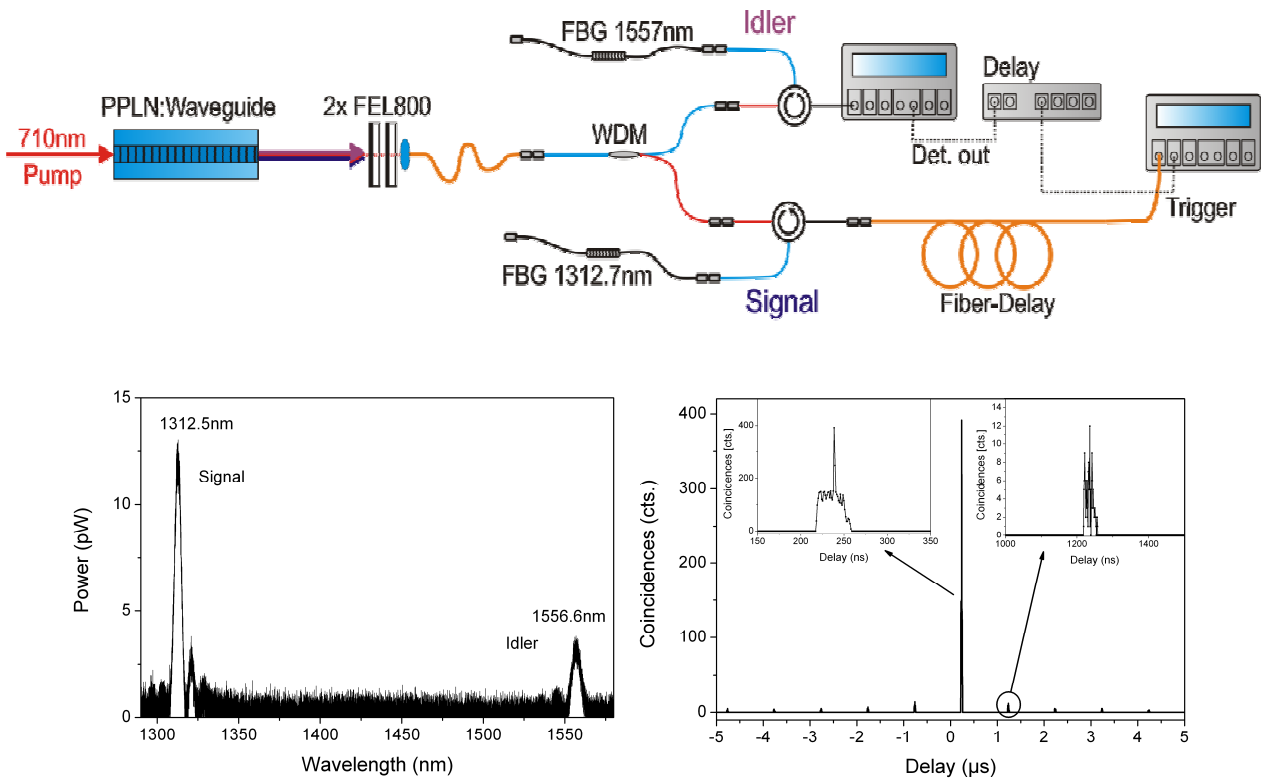


Figure 11: Experimental set-up (top), typical emission spectrum (bottom left) and correlation measurement results (bottom right).

By correlating the detection events of both detectors, the correlation between signal and idler photons was proven and at low pump power (approx. 100 μW) the background count rate is very small leading to a high correlation-to-accidentals ratio (CAR) of 97. Based on this, a heralded single-photon source at telecom wavelengths (1.3 μm , 1.55 μm) based on SPDC photon pairs was produced, see Figure 12. Parameters such as photon pair rates, heralded photon rates and heralding/Klyshko efficiencies were measured. Furthermore, first and second order coherence as well as photon statistics measurements have been performed.

Further improvements in the experimental setup, i.e. improved coupling efficiency from and to the nonlinear waveguide crystal, were performed and several parameters of the heralded single photon source at 1310/1550 nm could be improved considerably, such as photon pair rates, heralding efficiency, conversion efficiency etc. All required parameters have been measured again, notably photon statistics and heralded second order correlation function ($g^{(2)}$ -function) vs. pump power. Very high photon pair rates up to 10^7 s^{-1} (corresponding to 60 000 coincidences per second and μW), a high signal-to-background ratio of approx. $600 \mu\text{W}^{-1}$ and a very high heralding efficiency up to 64 % were measured. Furthermore, first and second order coherence as well as photon statistics measurements have been performed. Measurements of the heralded $g^{(2)}$ -functions vs. pump power yield an extremely small $g^{(2)}(0) = 0.001$ at 20 nW pump power, only limited by detector dark counts. The results are shown in Figure 13.

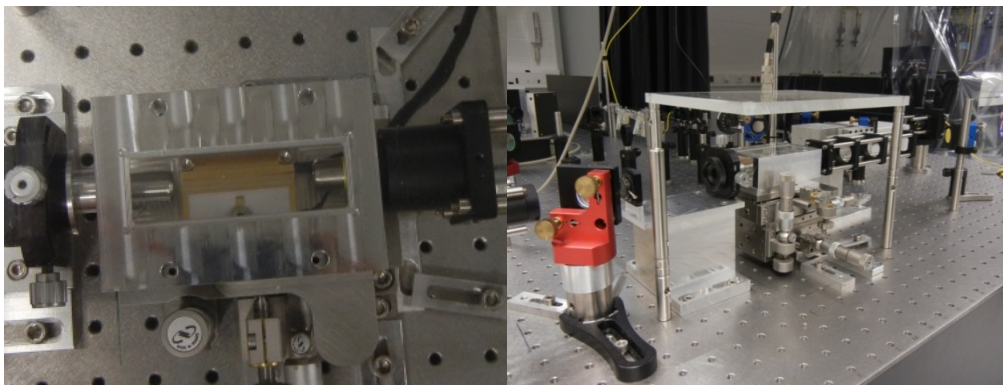


Figure 12: The heralded single-photon source at telecom wavelengths (1.3 μm , 1.55 μm)

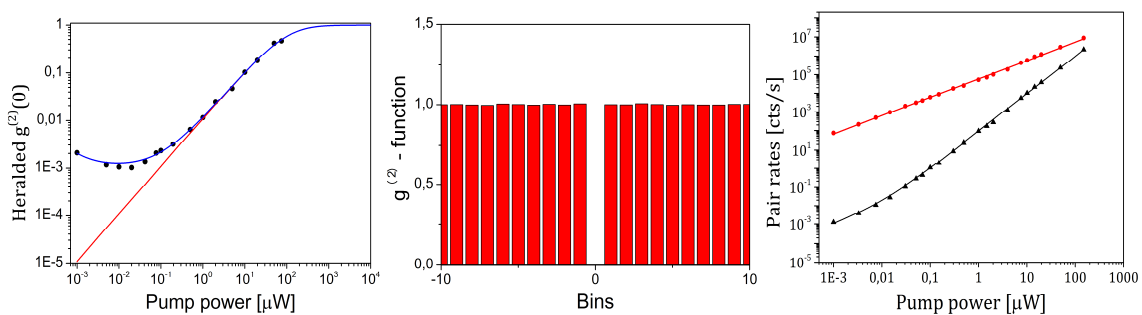


Figure 13: left) heralded $g^{(2)}(0)$ as a function of pump power; middle) $g^{(2)}$ of the heralded arm; right) pair rates as a function of the pump power.

The work on the heralded single-photon source at telecom wavelengths (1.3 μm , 1.55 μm) was finalized by measuring the photon indistinguishability. For the heralded single-photon source at telecom wavelengths (1.3 μm , 1.55 μm) based on SPDC photon pairs the indistinguishability (purity) of the photons was measured in a Hong-Ou-Mandel (HOM) interference experiment. The generation of pure photons requires a pulsed pump laser together with the two Fibre-Bragg-Gratings to eliminate spectral correlations. The purity is observed from the visibility of the HOM-interference of two signal photons from consecutive pulses. In the experimental setup, the signal photons are sent to a fibre-based Mach-Zehnder interferometer with a delay of the inverse repetition rate of the pump laser. The idler photons are detected as heralds to project the signal photons into a heralded single photon state. Hence, the HOM interference appears in the 4-fold

coincidence rate. The shape of the HOM interference dip was measured and the agreement with the first-order coherence function, as expected from theory, was validated. The visibility was measured as a function of the pump power and reaches high visibilities above 90% for low pump powers due to the absence of detector noise and multi-photon contributions.

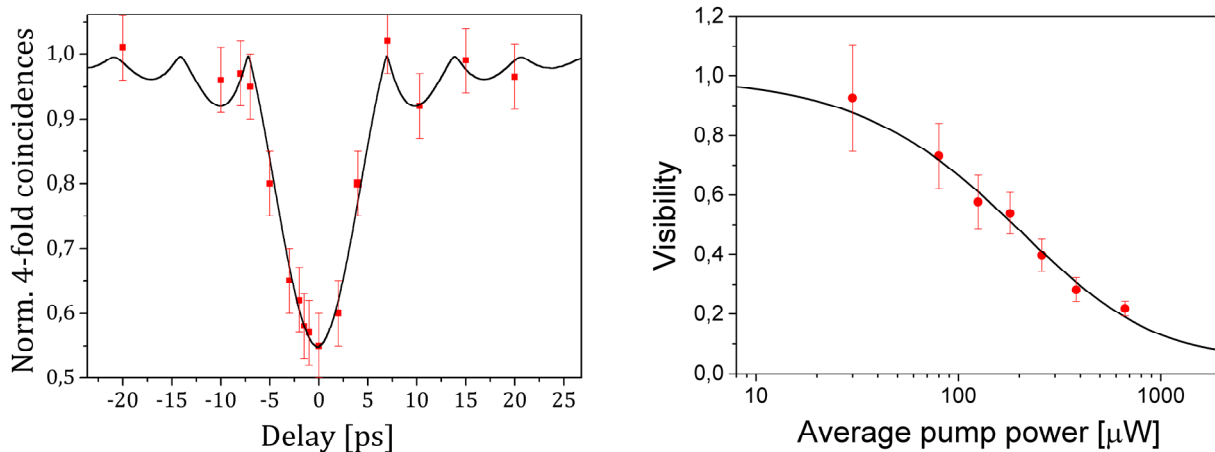


Figure 14: (left) coincidence measurement of subsequent photons under pulsed excitation of the waveguide photon pair source showing a Hong-Ou-Mandel (HOM) dip; (right) visibility of the HOM dip as function of average pump power, decreasing towards higher pump powers due to multi-photon contributions.

Characterisation of these single-photon sources by appropriate metrics in terms of wavelength, bandwidth, photon statistics, anti-bunching, and indistinguishability

Detailed results of the characterization of the single-photon sources were already reported in section 0 for the single-photon sources based on defect centres in nanodiamonds, based on semiconductor quantum dots and based on nonlinear effects in waveguides. This section is thus limited to additional characterizations of single-photon sources described in section 0 and for further sources, on which characterization procedures were carried out and which might be useful for characterization processes in general.

3.1.4 Single-photon sources based on defects centres in nanodiamonds

The single-photon emitters produced within the project but also from other manufacturers where characterized in terms of $g^{(2)}$ -value, spectral characteristics, photon statistics and photon flux. The SPSs to be characterized were originally planned to be based on colour centres (NV and SiV) in nanodiamonds to be produced using two distinct fabrication processes, i.e. based on chemical vapour deposition (CVD) and based on bead assisted sonic disintegration (BASD) method. During the project, the INRIM group, in collaboration with the University of Torino, has realized a single-photon-sensitive confocal microscopy facility at INRIM dedicated to the activities of the project, and in particular to the characterization of SPSs based on single colour centres in diamond and to their exploitation in quantum optics experiments. This activity has produced highly satisfactory results as testified by several publications on this subject. In *D. Gatto Monticone et al. Phys. Rev. Lett. 113 (14), 143602 (2014)*, the capability of performing full quantum optical characterization of the single-photon sources of interest for the project was shown [Ref. 6]. In *J. Forneris et al., Sci. Rep. 5, 15901 (2015)* [Ref. 20], a full quantum optical characterization of NV-centres in bulk diamond was performed, when these centres are stimulated by electrical injection. In *D. Gatto Monticone et al., New J. Phys. 16 (5), 053005 (2014)* [Ref. 1] and in *D. Gatto Monticone, et al., Int. J. Quantum Inf. 12, 1560011 (2014)* [Ref. 9] an extensive study on centres of a newly reported family of defects was performed. Those centres have spectral characteristics and lifetime that are compatible with the ones of the SiV-centres.

At PTB, the focus was on the NV-centre doped nanodiamonds. Diamond nanocrystals with NV-centres, produced by REG(UDS) on cover glass and in an antenna structure, delivered from REG(FAU) have been characterized in terms of wavelength, background, second order correlation function, $g^{(2)}(0)$ and count rate. The maximum count rate achieved was 700 kcps for nanodiamonds directly on glass and 2.9 Mcps for nanodiamonds on an additional MgF₂ intermediate layer. Lowest $g^{(2)}(0)$ -values were 0.06 for nanodiamonds

on glass and 0.34 for nanodiamonds in an antenna structure, which was produced by REG(FAU). The background count rates were 40 kcps and 250 kcps for nanodiamonds on glass and in an antenna structure, respectively. The spectral bandwidth was about 200 nm, as expected. In Figure 15, the confocal scan, a close-up of one nanodiamond, the emission spectrum and the second order correlation function for the sample exhibiting a photon rate of 960 kcounts/s, an emission lifetime of the NV-centre of ~ 17 ns, a $g^{(2)}(0)$ of 0.055 and a background count rate of 30 kcounts/s are shown.

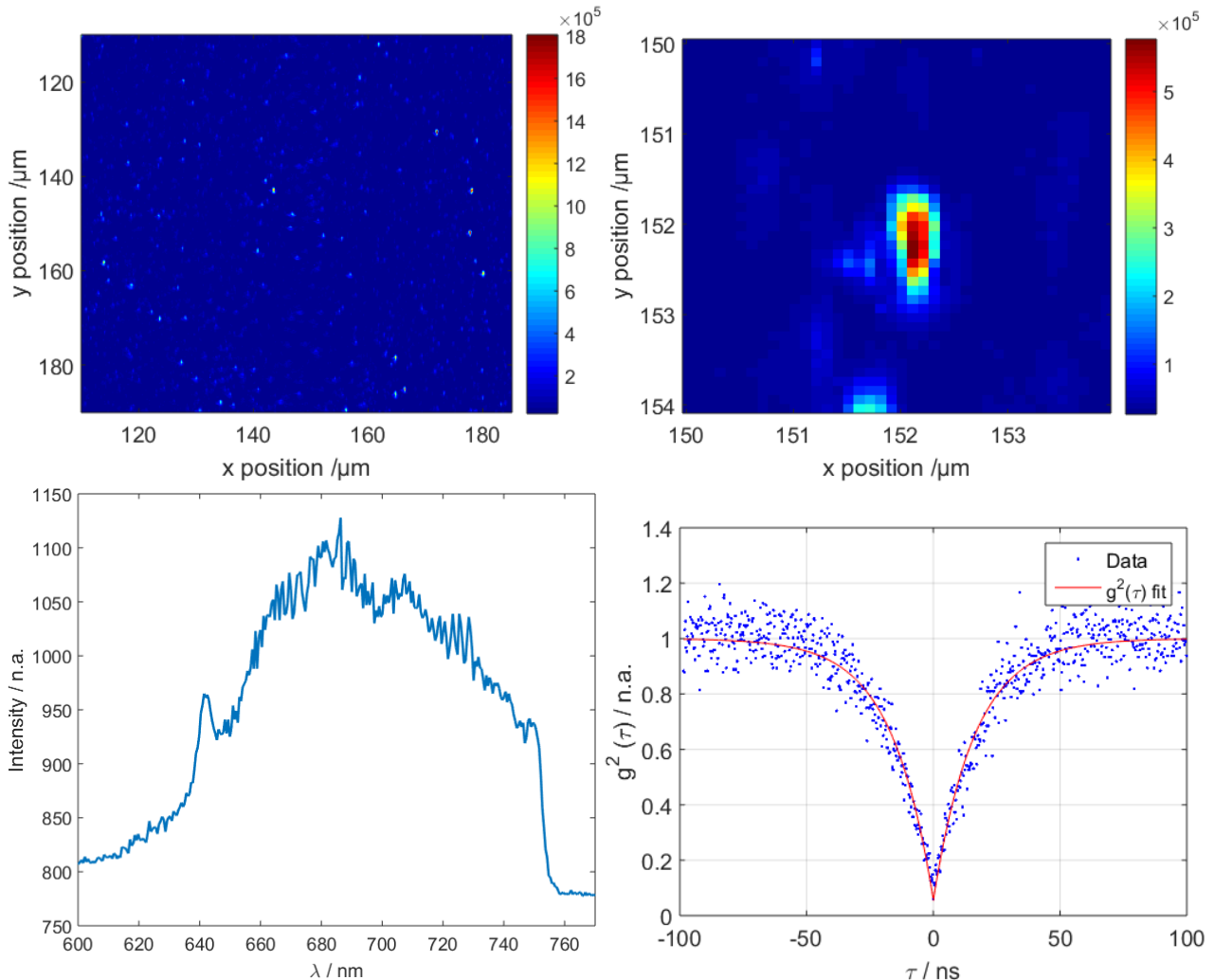


Figure 15: upper left) confocal scan, upper right) close-up scan of one nanodiamond, lower left) emission spectrum and lower right) second order correlation function for a NV-centre doped sample.

As stated, within this project a full quantum optical characterization of NV centres in bulk diamond, stimulated by electrical injection was performed by INRIM. Figure 16 shows the scheme of the single-photon electroluminescent device, in Figure 17 shows the luminescence spectra and the results of the 2nd order correlation function measurement, indicating the sub-classical nature of the emission [Ref. 20].

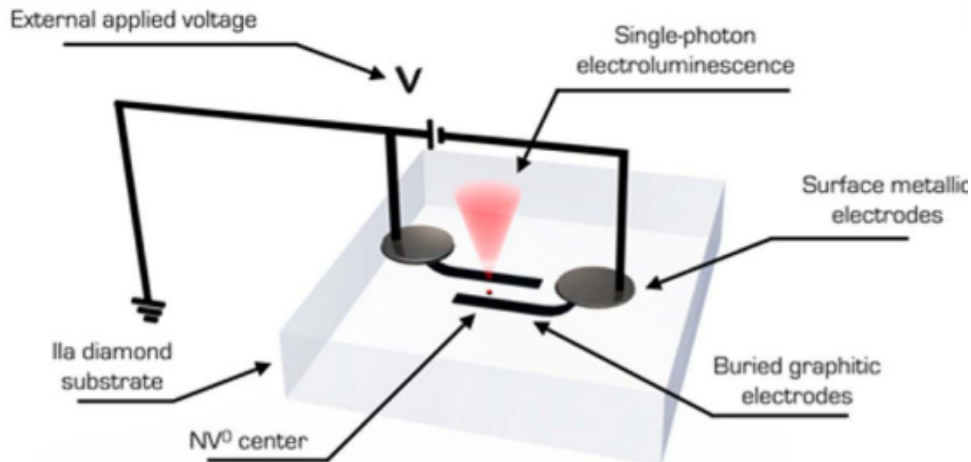


Figure 16: Scheme of the single-photon electroluminescent device. From Ref. 20.

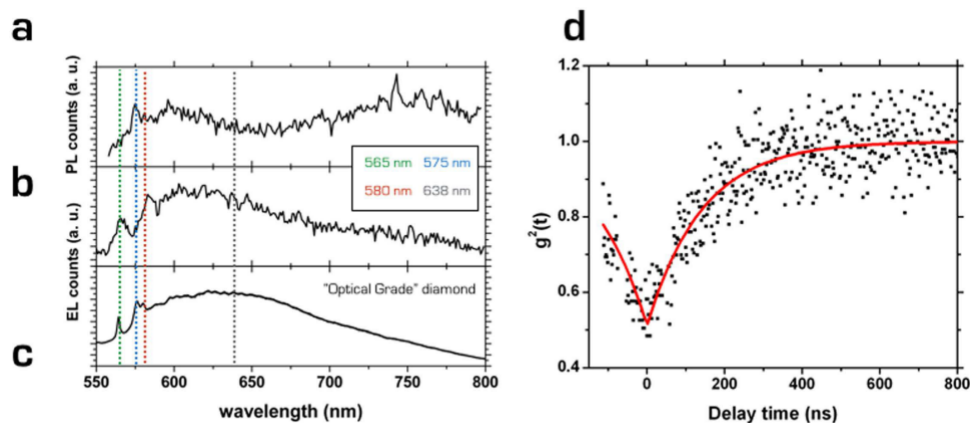


Figure 17: Non-classical electroluminescence (EL) emission. (a) PL ($\lambda = 532$ nm excitation) and (b) EL (240 V bias) spectra acquired (c) Reference EL spectrum acquired at 500 V applied bias from an “optical grade” device fabricated with a 6 MeV C^{3+} microbeam. (d) $g^2(t)$ curve acquired. The curve is not corrected by background removal. From Ref. 20.

3.1.5 Investigation of higher order correlation functions (g -functions)

Another focus of the work was the investigation of higher order correlation functions (g -functions). INRIM, in collaboration with partner USMF and the University of Torino, has realised two confocal microscopy systems working at the single photon level addressed to the characterisation of several single emitters and their exploitation as single photon sources.

The first system features an excitation wavelength of 532 nm (solid state laser) with a detection wavelength starting from 570 nm. The second system features an excitation wavelength of 692 nm with a detection wavelength starting from 730 nm. Both systems can be equipped of both air (NA=0.9) and oil (NA=1.3) objectives and their output is connected to a Hanbury-Brown & Twiss interferometer composed of a 50% / 50% beam splitter and two commercial SPADs (Single Photon Avalanche Diodes) addressed to the direct measurement of g^2 function via coincidence detection. The preliminary measurements performed on the samples carried out at INRIM; yield results in agreement with the known properties of the analysed emitters in terms of emission rate, wavelength and mean lifetime, demonstrating the good performance of our experimental systems.

Within this project, a multiport HBT interferometer for the measurement of $g^{(2)}$, and $g^{(3)}$ was realised at INRIM. A confocal microscope system (Figure 18) was upgraded to be able to perform $g^{(2)}$ and $g^{(3)}$, measurements in parallel with a detector tree and super-resolution imaging. The device has been realized and used for experiments connected to mode structure reconstruction of optical states and sub-diffraction

imaging of colour centres in diamond. Several experiments related to high order g -functions by the multipoint Hanbury-Brown and Twiss interferometer for the characterisation of sources have been performed at INRIM and at PTB. At INRIM, with support from USMF, in specific the mode reconstruction to super resolved confocal microscopy of SPS was carried out. An interferometer system for the measurement of multi-dimensional time-resolved $g^{(2)}$ was realised and multi-dimensional time-resolved $g^{(2)}$ characterisation of single-photon sources were performed. In specific, the work describes the results obtained in INRIM regarding the realization of a novel technique for the characterization of SPSs based on the study of the temporal dependence of the statistical properties of those objects. In particular we have performed a two-times $g^{(2)}$ measurements, where the reference is given by the laser pulse and the “two-times” are the time tagging of the clicks by the two detectors. This technique can provide useful insight on the non-classical properties of SPSs that find successful exploitation in quantum information protocols. The SPSs in this experiment were based on NV centres in nanodiamonds (dimension: up to 250 nm in diameter). The $g^{(2)}$ plot was analyzed by USMF and INRIM, it clearly shows the presence of a dip corresponding to the three-fold coincidence between the laser pulse and the two detectors, as expected for the behaviour of a SPS.

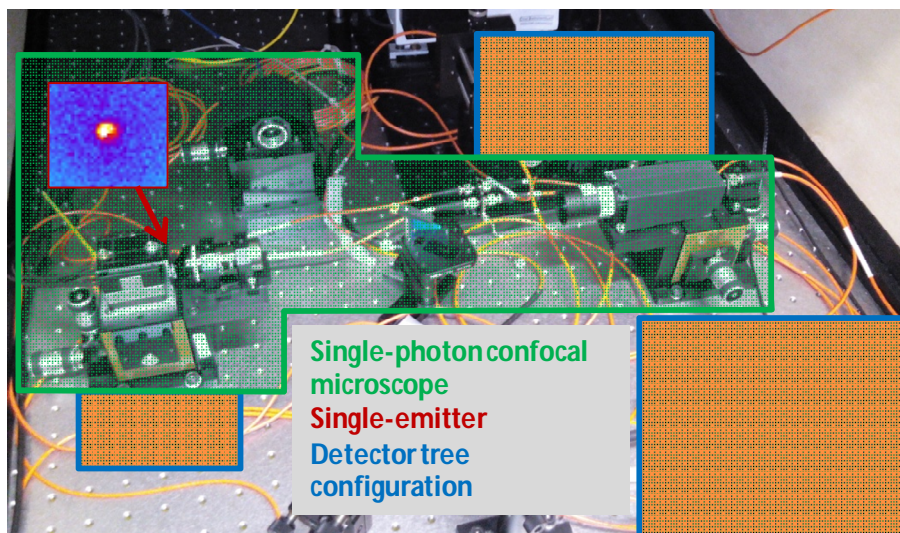


Figure 18: Single-photon confocal microscope with detector tree for $g^{(2)}$, $g^{(3)}$ and $g^{(4)}$ measurements.

Development of an excitation scheme with adjustable frequency allowing for traceable photon flux measurements

3.1.6 Low optical flux detector

A transfer standard detector system, called LOFDS (Low optical flux detector for SIQUTE) able to measure 50 fW with an uncertainty below 1 % at the wavelength range from 650 nm to 750 nm was designed and realized by CMI. It consists of a low noise low dark current Si detector (Hamamatsu S1227 33 BR) in conjunction with a custom-made switched integrator amplifier (SIA), see Figure 19. The SIA has a conversion factor as high as 10^{12} and in conjunction with the Hamamatsu S1227 33 BR Si photodiode, the noise level measured can be as low as 1 fW/Hz^{1/2} which corresponds to ≈ 4000 photons/Hz^{1/2} at a wavelength of 750 nm. A series of noise performance measurements were performed with the transfer standard detector. The noise equivalent power in dark conditions has been measured to be as low as 1 fW/Hz^{1/2} (~ 3500 Photons/s) with 2 seconds integration time and for photons wavelength of 700 nm. Furthermore, Allan deviation analysis, see Figure 20 has shown that the main noise contribution up to 100 s is white noise which means that by using longer integration time it is possible to further reduce the noise: a measurement time of 100 s leads to a standard deviation as low as 400 photons/s (@700nm).

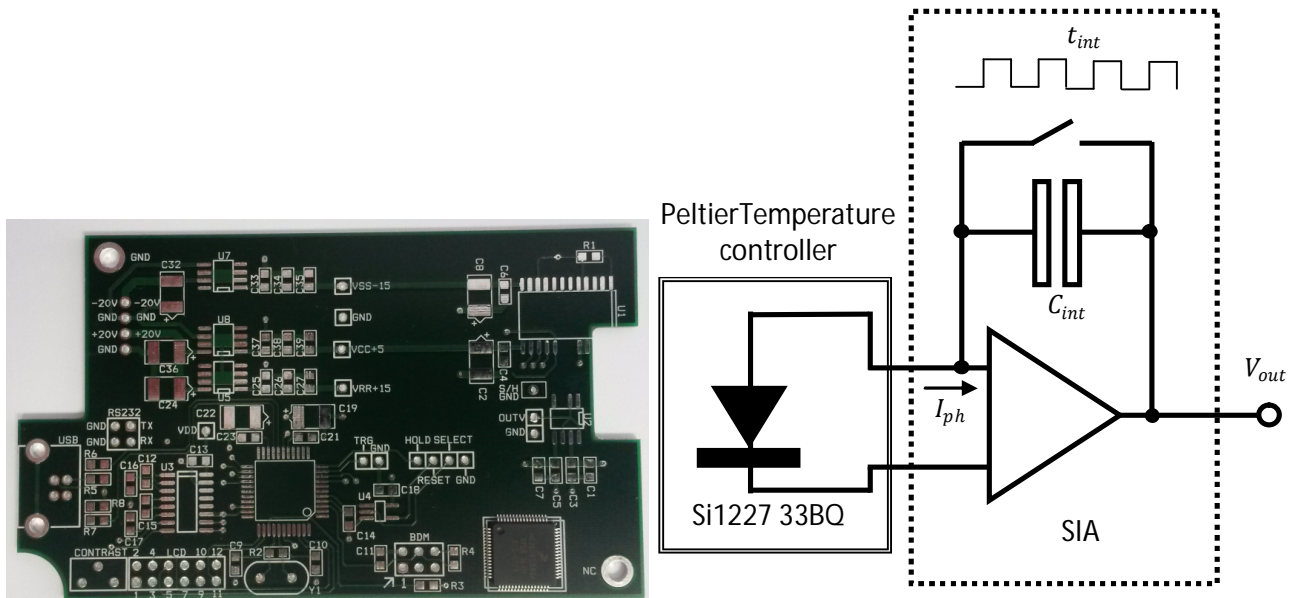


Figure 19: left) the Switched-Integrator Amplifier board, right) the simplified scheme of the CMI reference detector for low photon fluxes (LOFD)

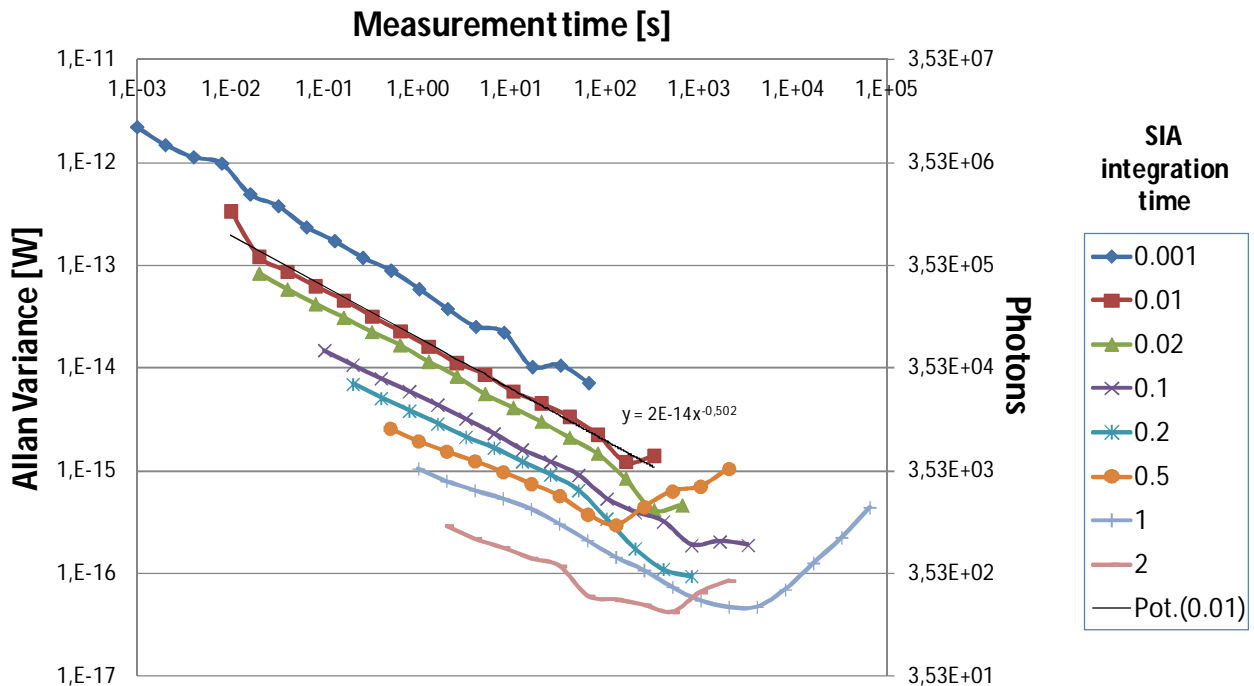


Figure 20: Allan variance as a function of measurement time for different integration times of the SIA.

The complete detection system was calibrated by CMI at 100 μ W power level using a 3-element trap detector transfer standard directly traceable to the cryogenic radiometer optical primary standard, the results are shown in Figure 21. Its linearity was measured using the absolute beam addition technique down to sub-pW power level.

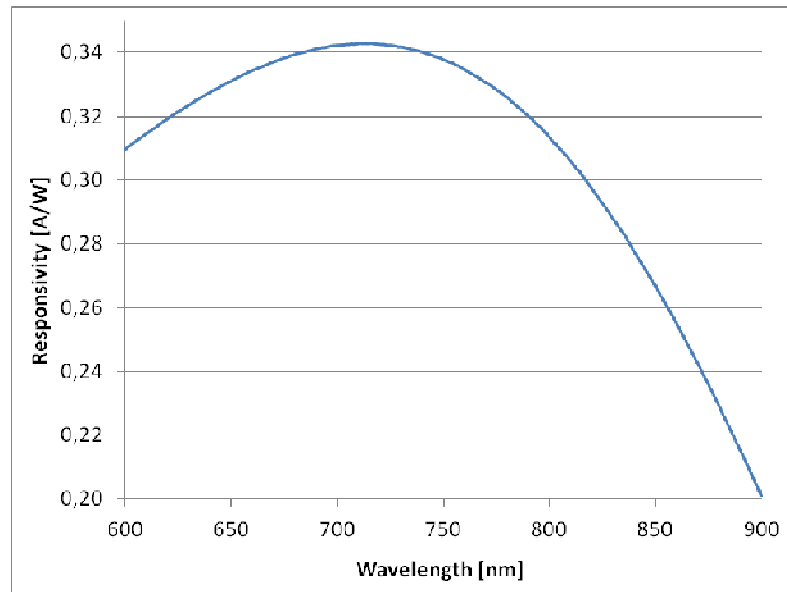


Figure 21: Spectral responsivity of the LOFDS.

With the LOFDS, an attenuated laser beam at 676 nm has been then measured from 50 fW to 10 pW with the transfer standard using an integration time of 1 s. For a moving average of 20 samples the standard deviation of the signal is below 1 % in all power ranges.

3.1.7 Multi-element tunnel type detector

Within this project, a multi-element tunnel type attenuator with 6 decades beam attenuation for the wavelength range 650 nm – 750 nm was designed and manufactured by Metroser. This device is based on the predictable reflectance of Si-photodiodes (Hamamatsu 1337-1010BQ). The number of photodiodes in the device is twelve, which results in a beam attenuation of approx. $2 \cdot 10^6$. The attenuator is shown in Figure 22.

The exact transmission of this device was measured at CMI with the LOFDS device described in section 3.1.6. At 676 nm, the transmittance of the attenuator is $T = 5.48 \times 10^{-7} \pm 5\%$. The attenuator performance is independent from polarization state, and the incoming and exiting beams are coaxial.

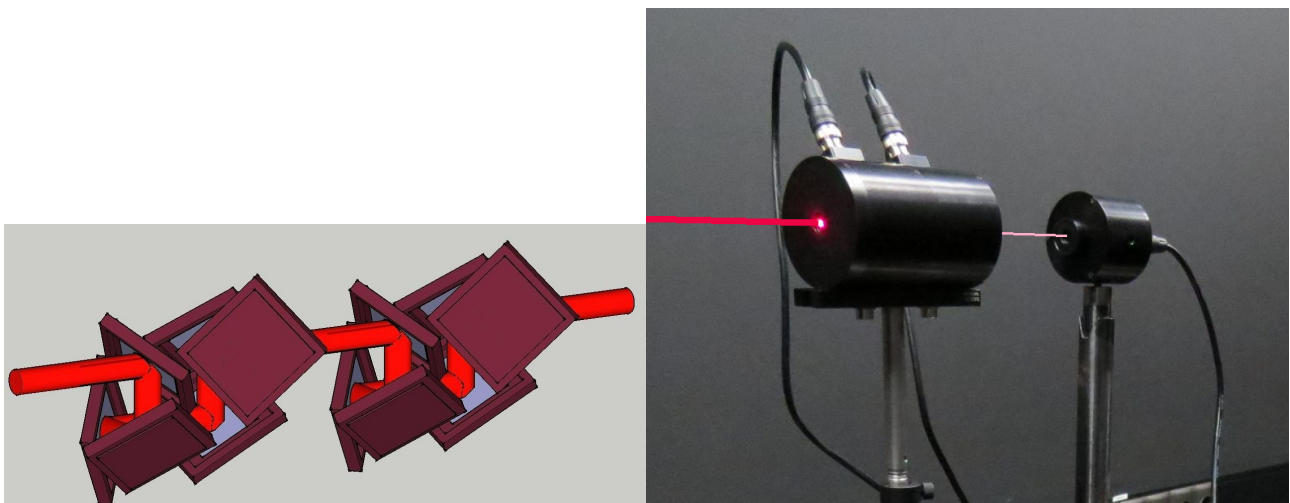


Figure 22: left) Illustration of the 12-element attenuator for six decades beam attenuation; right: The high-attenuation tunnel-type detector for calibration of single-photon devices (top).

3.1.8 Adjustable repetition rate excitation scheme

A pulsed diode laser at a wavelength of 685 nm with an adjustable frequency ranging from 100 kHz to 80 MHz and pulse width of 40 ps to 50 ps (FWHM) was designed, realized and characterized by MIKES. This device is later used for the frequency-dependent excitation of a single-photon emitter based on SiV-centre doped nanodiamonds.

The output of the pulsed diode laser was characterized with the measurement setup shown in Figure 23. The laser optical output (laser head PiL069XSM with controller) was connected via a polarization maintaining single mode fibre to an ultrafast InGaAs photodiode (New Focus Model 1014). The InGaAs-detector is sensitive from 500 nm up to 1630 nm. At 685 nm the response is about 0.23 A/W. The bandwidth (at -3dB) of the detector is 45 GHz and typical rise time 9 ps. The electrical signal from the photodiode was acquired with a 20-GHz oscilloscope (Agilent 86100A). The waveforms were recorded and analysed. The laser head was attached to breadboard for better thermal stability.

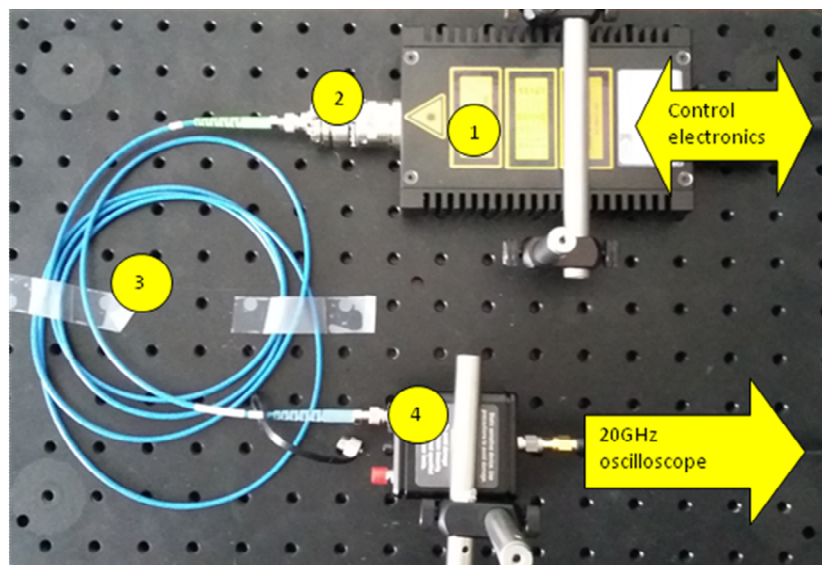


Figure 23: The measurement setup to characterize the laser. 1 – the PiL069XSM laser head, 2 – fibre port, 3 – single mode polarization maintaining fibre, 4 – New Focus Model 1014 InGaAs-photodiode

The average energy of the pulse was calculated from the average power at the fibre output divided by the laser repetition rate. The average pulse energy is varying between 8 pJ and 10 pJ for laser repetition rates between 10 MHz and 80 MHz, see **Error! Reference source not found.**

Repetition rate (MHz)	80	70	60	50	40	30	20	10
Pulse width FWHM (ps)	44	40	44	43	48	48	50	50
Pulse energy (pJ)	9,5	10,3	9,7	9,4	8,7	8,4	7,8	7,7

Table 1: Characteristics of excitation pulses directly after 1 m of polarization maintaining single mode fibre. The pulse width is measured with an oscilloscope (Agilent 86100A) and 45 GHz bandwidth photodiode (New Focus 1014) using an optical attenuation to limit the input power. The pulse energy is characterized with a Si photodiode in conjunction with a custom made switched integrator amplifier. The relative uncertainties for both measurements are below 1% and they are negligible relative to other uncertainty components affecting the photon flux measurements.

The stability and repeatability of optical pulses were characterized by analyzing the pulse waveform, from which the pulse area and thus the pulse energy and the pulse peak power can be derived. Figure 24 shows

a typical pulse at 70 MHz repetition rate. The short-term stability is affected by a combination of pulse to pulse deviation and electronic noise in the measurement equipment and leads to a short-term noise of approx. 4 %. The long term stability is affected largely by the temperature stability of the laser head. For analysing the long term stability the Allan deviation analysis was used. The results are shown in Figure 25.

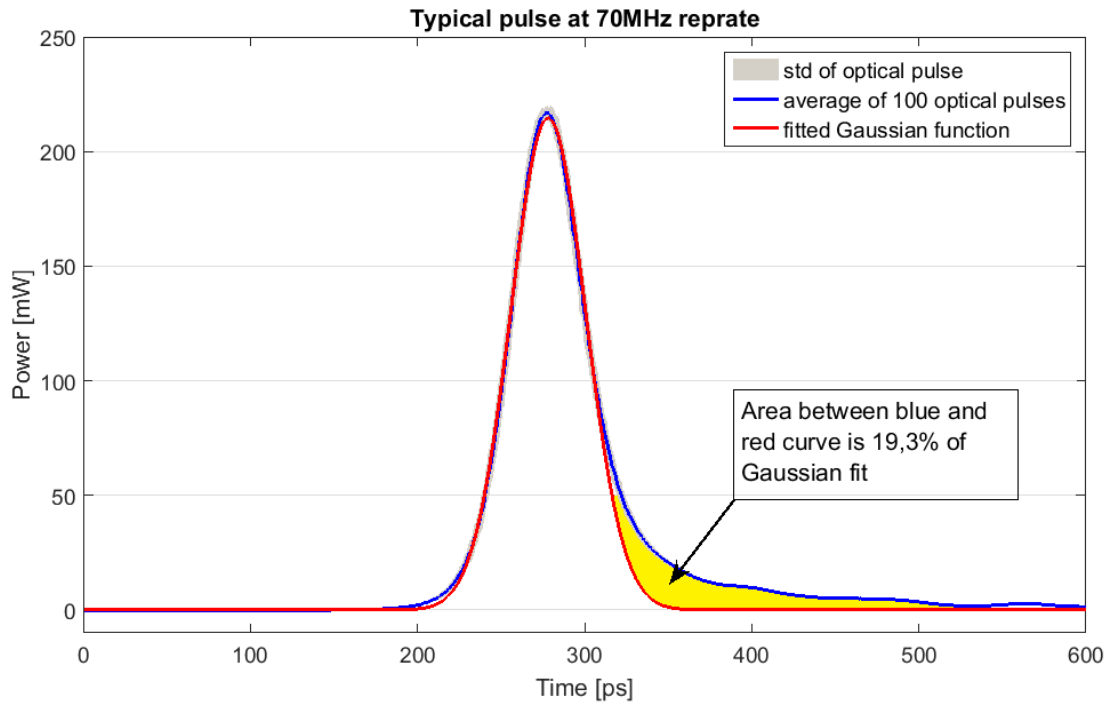


Figure 24: Typical pulse shape and deviation from the ideal Gaussian-shaped pulse shape for a repetition rate of 70 MHz.

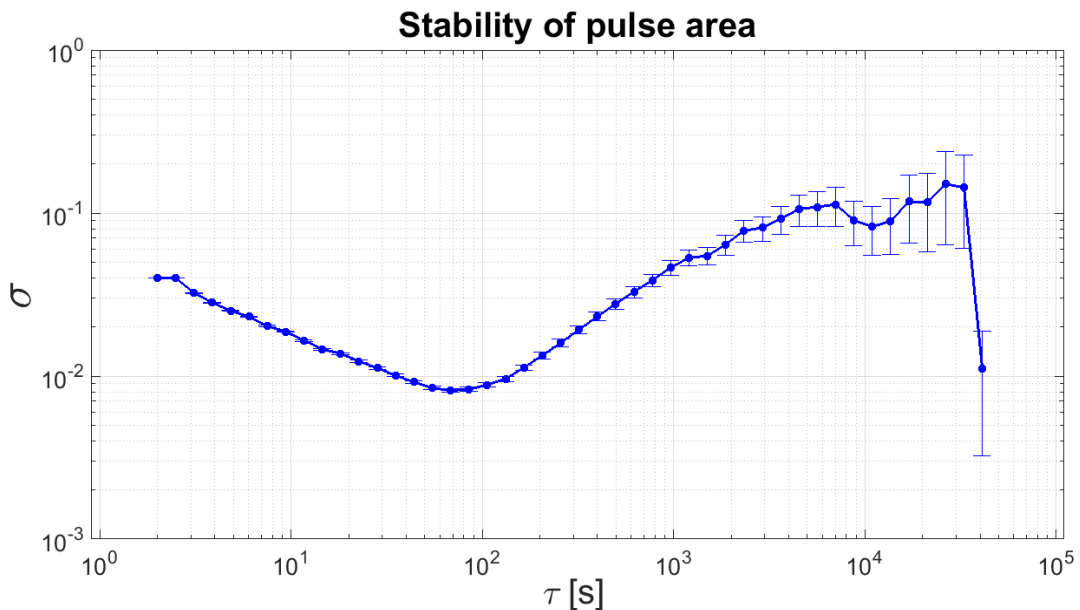


Figure 25: Long term stability of the pulse area. The standard deviation σ for different averaging times τ . The best averaging time is around 1 minute.

3.1.9 Traceable low-photon flux measurements

The absolute optical power of the SiV-centre was directly measured at REG(FAU) in cooperation with CMI and MIKES with the beyond the state of the art absolutely calibrated photodetector developed within this project, see sections 3.1.6 and 3.1.8. A linear behaviour with respect to the repetition rate of the pump laser was observed, see Figure 26.

The aim of the work was to test the application of the developed and characterized sub-ns pulsing diode laser system for excitation of the single-photon source. The single-photon source is a SiV colour-centre in a nanodiamond, provided by REG(UDS) and implemented into a dielectric structure by REG(FAU). The operating wavelength of the laser was 685 nm that is the optimum for pumping SiV-centres. The lifetime, photoluminescence spectrum and coincidence of bright SiV-centres were measured. At first, the repetition rate of the pump laser was set to maximum and the optical power was measured by the photodetector mentioned above. Based on the measured optical power and known wavelength the absolute photon flux was calculated. Later the repetition rate of the pulsing laser was reduced. A linear behaviour with respect to the repetition rate of the pump laser was observed. This method is promising and the tests show its potential for the application of the developed excitation scheme for the characterization of the photon flux of single-photon sources as well as for the calibration of single-photon detectors using single-photon sources (see Figure 26). An article presenting the abovementioned results was published in *Metrologia* (Aigar Vaigu *et al* 2017 *Metrologia* 54 218-223 [Ref. 28]).

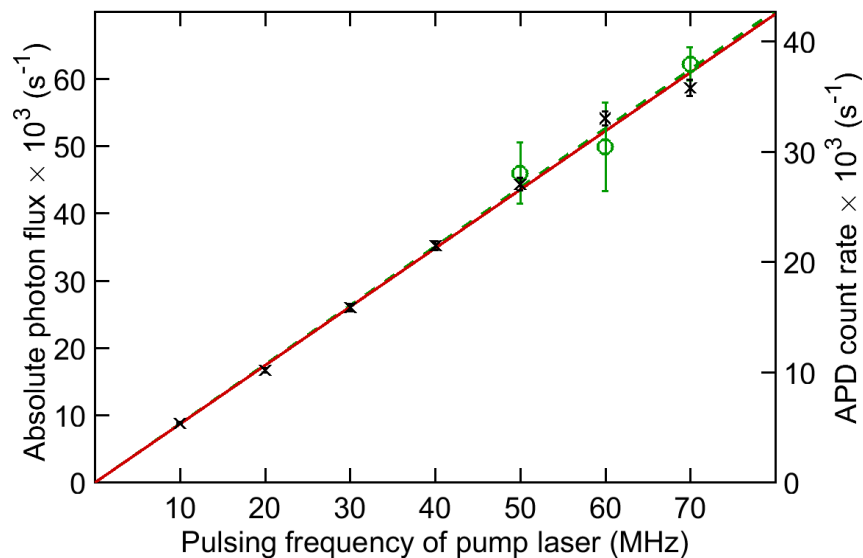


Figure 26: Photon flux as a function of the pump laser repetition frequency. The photon flux of the silicon vacancy centre in a nanodiamond was measured at 50–70 MHz of pump frequency with an absolutely calibrated silicon photodetector (circle symbols, left vertical scale). The avalanche photo diode (APD) count rates (cross symbols, right vertical scale) are shown for the whole frequency range from 10 MHz up to 70 MHz. Both measured photon fluxes are fitted with a straight line passing through the origin. The total efficiency of the source $(0.88 \pm 0.10) \times 10^{-3}$ is given by the slope of the absolute photon flux (circle symbols, dashed line), while the slope for the APD count rate is $(0.54 \pm 0.02) \times 10^{-3}$ (cross symbols, solid line). The slope for the APD count rate differs from the slope of the absolute photon flux by a factor of 0.61, which is the quantum efficiency of the APD (this result agrees with the nominal value stated for the APD). The results are presented with expanded uncertainties i.e. with a level of confidence of approximately 95%.

Within the frame of this project, also a comparison between the LOFDS detector developed at CMI and the double attenuator technique, developed at PTB, was carried out, see *G Porrovecchio et al., Metrologia 53 (2016) 1115–1122* [Ref. 24]. This comparison was carried out down to sub-100-fW optical power level between a low-noise Silicon photodiode and a low optical flux measurement facility based on a double attenuator technique. The comparison was carried out via a Silicon Single-Photon Avalanche Diode (Si-SPAD), which acted as transfer standard. The measurements were performed at a wavelength of 770 nm using an attenuated laser as radiation source at optical power levels between approx. 86 fW and approx.

1325 fW, corresponding to approx. 330000 photons per second and approx. 5.2×10^6 photons per second, respectively, see Figure 27. The mean relative deviation of the detection efficiencies of the Si-SPAD, determined by the Si-photodiode and the low optical flux measurement facility, i.e. between two completely independent traceability routes, was $< 0.2 \%$, see Figure 28, thus well within the combined standard uncertainty of the two measurements. To our knowledge, this is the first comparison for the detection efficiency of a single photon detector using a direct optical flux measurement by a conventional Si-photodiode at such low power levels.

A guideline on the detection efficiency calibration of Si-SPAD detectors and on an alignment procedure for Si-SPAD detectors was written by PTB and uploaded to the SIQUTE website.

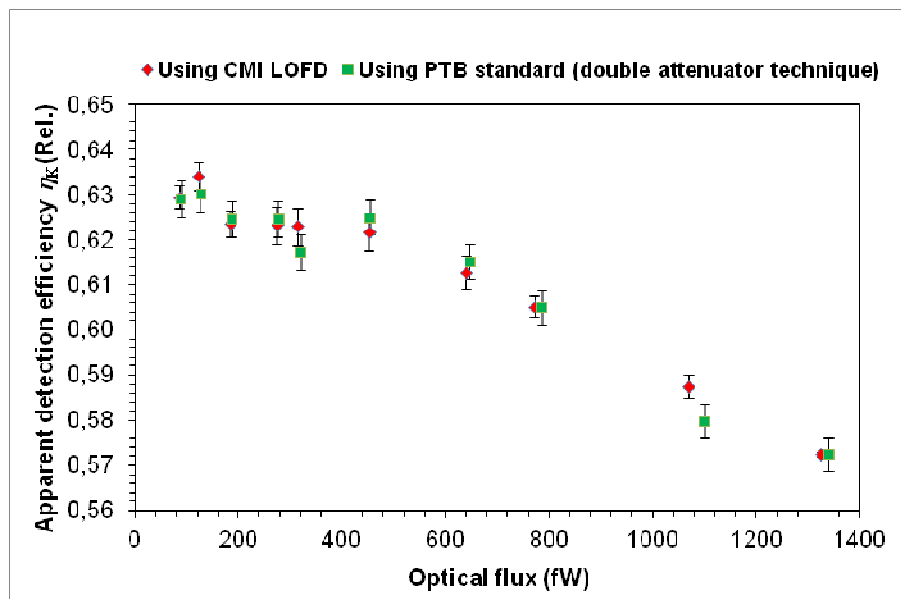


Figure 27: Results of the comparison of the detection efficiency of a Si-SPAD detector with the PTB low flux measurement facility and the CMI low flux standard detector.

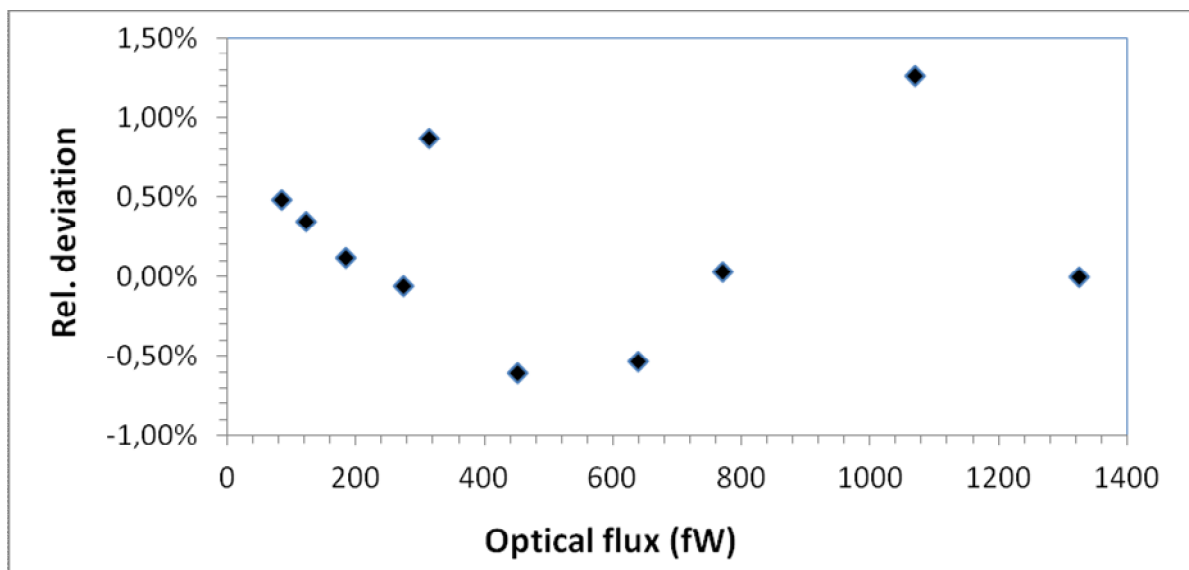


Figure 28: Deviations between the detection efficiency calibrations of the Si-SPAD detector for different count rates.

Demonstration of the suitability of single-photon sources for different entanglement enhanced measurements

In order to demonstrate the suitability of single-photon sources for different entanglement-enhanced measurements, first a theoretical study on quantum states of light (squeezed light, NOON states, twin beams) and on quantum correlation techniques were performed in order to preliminarily identify possible quantum-enhanced measurement experiments. Four innovative protocols exploiting non-classical photon number statistics and correlation were analyzed, i.e. Sub-Shot-Noise Imaging with SPSs, Ancilla assisted target detection in a noisy environment, Microscopy super-resolution by exploiting Glauber $g^{(k)}$ functions and Phase correlation measurement in coupled interferometers via Squeezed states.

3.1.10 Quantum-enhanced resolution in confocal fluorescence microscopy

Quantum-enhanced resolution in confocal fluorescence microscopy obtained by exploiting the non-classical photon statistics of single nitrogen-vacancy colour centres in diamond was experimentally demonstrated, see Ref. [6]. This was achieved by developing (INRIM) a general model of super-resolution based on the direct sampling of the k^{th} -order autocorrelation function of the photoluminescence signal. This model shows that it is possible, in principle, to resolve arbitrarily close emitting single-photon emitters, see Figure 29.

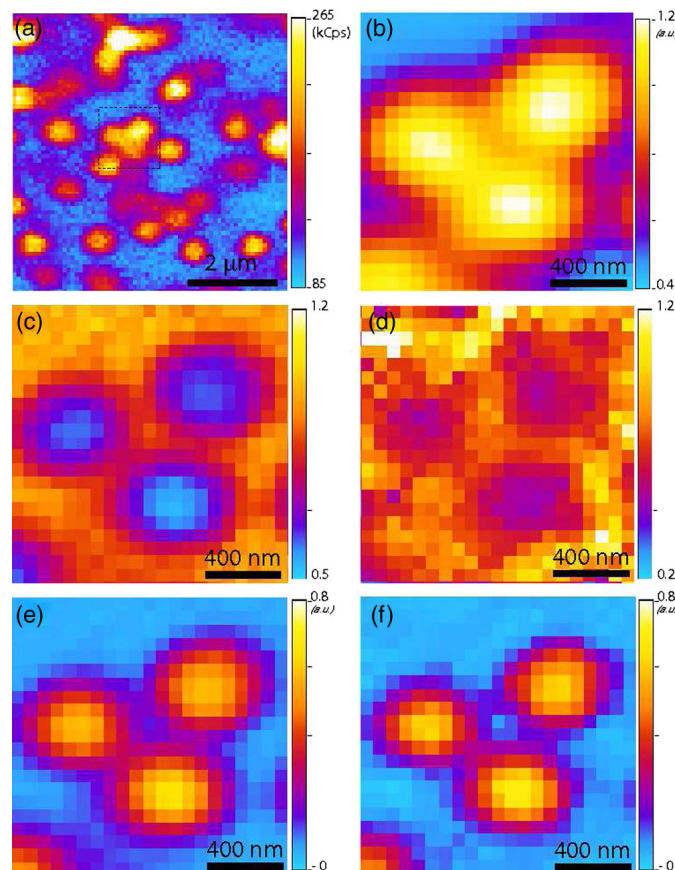


Figure 29: Example of the super-resolution technique applied to a cluster of 3 NV centres. (a) Typical scan of a region of the sample obtained by collecting the signals emitted by each centre on a pixel-by-pixel basis via a single-photon sensitive confocal microscope. (b) Magnification of the area of interest. (c) Map of g^2 -function. (d) Map of g^3 -function. (e) Super-resolved map for $k = 2$. (f) Super-resolved map for $k = 3$.

3.1.11 Innovative quantum techniques for the characterisation of quantum networks

An intensive experimental study on a novel protocol (inspired by *Hradil et al., New J. Phys 14, 095001 (2012)* and references therein) was completed by INRIM with support from NPL (*F. Piacentini et al., "Towards joint reconstruction of noise and losses in quantum channels", Quantum Measurements and Quantum Metrology. 3, No. 1, 27–31, (2016)*), which should allow one to simultaneously reconstruct the

statistical properties of an unknown quantum state, and the detection efficiency of the measurement apparatus (in particular, a photon number resolving detector). For a known detection efficiency, this enables the measurement of the optical channel transmittance, since the overall detection efficiency is due to the channel loss and detector efficiency. The experiment was performed using the almost noiseless heralded single-photon source (HSPS) described in *Brida et al., Appl. Phys. Lett. 101, 221112 (2012)* and the transition-edge sensor (TES) detector, see *Lolli et al., Intl. J. Quant. Inf. 9, Suppl.; 405-413 (2011)*. The data enabled a faithful reconstruction of the photon number distribution only up to 2 photons, but showed good reconstruction measurement of transmittance. It is believed that these unsatisfactory results are due to poor optical coupling out from the HSPS and the low detection efficiency of the TES detectors, leading to noise dominating the measurement data. Improving the performance of the experimental setup was not achievable within the lifetime of the project. The study nevertheless provided useful insights on how to characterize quantum networks. The method studied generally works well for realistic scenarios when the characteristics of the optical systems are close to ideal, but does not provide very useful information in the presence of a significant/dominant level of inefficiencies and losses.

3.1.12 Single SPDC pair source pumped and demonstration of entanglement

A source of wavelength-degenerate (1584 nm), polarization-entangled states $|\Psi\rangle = |V_1H_2\rangle + e^{i\phi} |H_1V_2\rangle$ was realized at NPL, see Figure 30. The setup utilizes a cavity which enhanced the pump power by an order of magnitude, and enabled bi-directional pumping of a periodically-poled KTP crystal. An interferometer is used to coherently entangle the down-converted states. The source has an 'open' architecture, enabling one to systematically perturb the properties of the state in order to evaluate the sensitivities when used for specific applications.

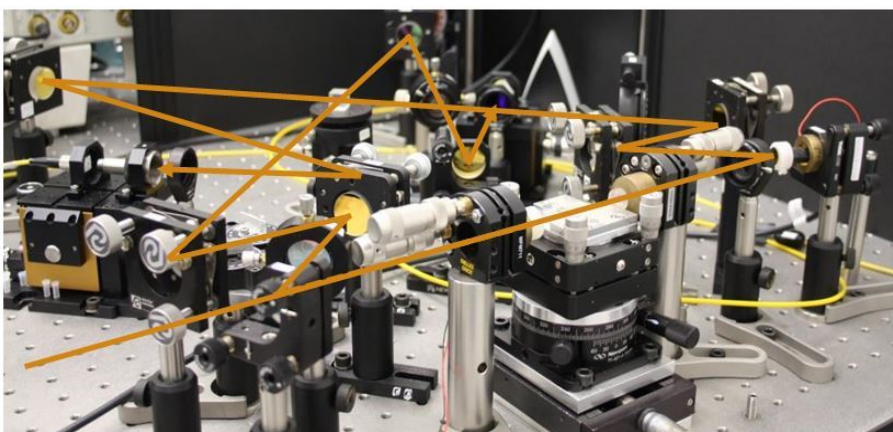
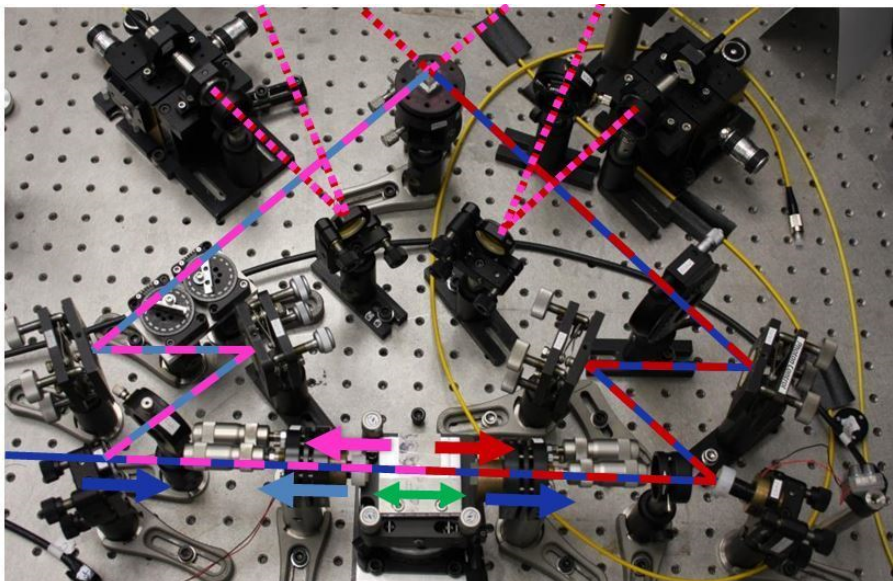


Figure 30: Plan and side view of pump-enhanced down-conversion source. Plan view: pump light (dark blue) enters the pump-enhancement cavity (green) from left. The transmitted pump light and forward-pumped down-converted photons (red) continue to the polarising beam-splitter at the apex of the external (Christmas tree) cavity and thence to fibre-couplers via two folding mirrors (one off-picture). The reflected pump light (light blue) and reverse-pumped down-converted photons (pink) travel to the beam-splitter in the reverse direction. The reflected and transmitted pump light is used to stabilise the Christmas tree cavity. Side view: Optical paths shown.

The polarization-entangled state $|\Psi\rangle = |V_1H_2\rangle + e^{i\phi} |H_1V_2\rangle$ was confirmed by measurements showing that:

- (i) the $|V_1H_2\rangle$ and $|H_1V_2\rangle$ photons are indistinguishable, the probability amplitude of $|\Psi\rangle$ being the sum of the probability amplitudes for $|V_1H_2\rangle$ and $|H_1V_2\rangle$ photons. Otherwise, the probability of $|\Psi\rangle$ would be the sum of the probabilities for $|V_1H_2\rangle$ and $|H_1V_2\rangle$;
- (ii) upon changing the phase factor ϕ to $\phi+180^\circ$, the phase of the coincidence variation with detector polarization also changed by 180° . This shows that the terms $|V_1H_2\rangle$ and $|H_1V_2\rangle$ are coherent (necessary for entanglement), otherwise there would be no dependence on ϕ ;
- (iii) the classical limit ($S \leq 2$) of the Clauser-Horne-Shimony-Holt (CHSH) Bell inequality was violated by more than 8 standard deviations. We estimate lower limits with 84% confidence on the Singlet (Mayers-Yao) Fidelity of the entangled state ($\geq 90\%$) and the Entanglement of Formation (≥ 0.51) using the methods of Bardyn et al. [Phys Rev A 80, 062327 (2009)].

A numerical analysis was developed by NPL and INRIM, which showed that the state described in (iii) above was not a pure entangled state, but a quantified mixture of the 4 possible polarization-entangled states, this mixture being dependent on the controllable experimental parameters of the set-up.

The source was used to measure polarization dispersion in polarization-maintaining optical fibre, which has stress-induced birefringence introduced into it. Correlated photons have previously enabled this measurement to be performed in a process requiring two separate measurements. The source developed in this project enables the same information can be obtained from a single measurement. Obtaining data of sufficient quality to make a clear comparison with classical techniques was not achieved within the lifetime of this project, but continues to be pursued with the aim of future publication.

This work has produced a source of entangled photons which will be used for future work to exploit these non-classical correlations for metrology; the investigation of polarization dispersion is laying the groundwork for further exploitation of such a source for characterizing telecom wavelength optical components.

Summary of the key results and conclusions of the research undertaken

In the following, the key results of this project are listed. It should be noted, that these results have been only possible to be achieved by a combined effort of the consortium and REGs of this project, see also the detailed descriptions above.

- o Dielectric antenna structures were successfully designed. All of them work according to their design. These structures contain single NV-centres and single SiV-centres. In addition to the work on the impurity-based nanodiamonds, also a metal-dielectric antenna design with a collection efficiency exceeding 99% of the emitted photons from single colloidal quantum dots was successfully realized, see X.-L. Chu et al., *Optica* 1, 203 (2014). The developed structures will be used by other NMIs, but also universities and research institutes for future work on efficient single-photon sources.
- o Diamond nanocrystals with NV-centres on a cover glass and in an antenna structure have been characterized. The photon rates achieved were 700 kcps for nanodiamonds in glass with a $g^2(0)$ -value as low as 0.06 and 2.9 Mcps for nanodiamonds in an antenna structure with a $g^2(0)$ -value of 0.34.

The nanodiamonds will be used in other NMIs for further work on single-photon sources.

- o A high-attenuation tunnel-type detector for calibration of single-photon devices was and a Switched-Integrator Amplifier (SIA) were manufactured. Both will be part of the new measurement facility developed with the goal of performing traceable calibrations of very low photon fluxes. The

transmittance of the attenuator is $T = 5.48 \times 10^{-7} \pm 5 \%$. The SIA has a conversion factor as high as 10^{12} and in conjunction with a small area, state of the art Si photodiode the noise level measured can be as low as $1 \text{ fW/Hz}^{1/2}$ which corresponds to ≈ 4000 photons $/\text{Hz}^{1/2}$ at wavelength of 750 nm. The attenuator will be used by other NMIs for high precision measurements.

- A transfer standard detector for the measurement of very low optical fluxes was realised. The noise equivalent power in dark conditions has been measured to be as low as $1 \text{ fW/Hz}^{1/2}$ (~ 3500 Photons/s) with 2 seconds integration time and for photons at a wavelength of 700 nm. Furthermore, Allan deviation analysis has shown that the main noise contribution up to 100 s is white noise which means that by using longer integration time it is possible to further reduce the noise: A measurement time of 100 s leads to a standard deviation of mean as low as 400 photons/s (@700nm). The standard detector will be used in other NMIs and possibly in industry.
- The attenuated laser beam at 676 nm has been then measured from 50 fW to 10 pW with the transfer standard described above using an integration time of 1 s. For a moving average of 20 samples, the standard deviation of the signal is below 1 % in all power ranges. Measurement shows the feasibility of the attenuator and the transfer standards detectors described above.
- The absolute optical power of the SiV-centre was directly measured with a beyond the state of the art absolutely calibrated photodetector down to photon rates below 100 000 photons per second. A linear behaviour with respect to the repetition rate of the pump laser was observed. The experiment is a first step towards a scalable single-photon source to be used in radiometry.
- The successful comparison between a low-noise Silicon photodiode and a low optical flux measurement facility based on a double attenuator technique down to sub-100-fW optical power level was the first comparison of this kind. The agreement between these measurements shows the metrological excellence of the involved NMIs, because completely different traceability routes were used. The comparison shows the excellence in the measurement capabilities of the involved NMIs in low-flux radiometry.
- For the first time to our knowledge, a single-photon source was absolutely metrological characterized with respect to its radiometric properties, i.e. photon flux, spectral photon flux, emitted absolute power and emitted absolute spectral power. The experiment is a first step towards a deterministic single-photon source to be used in radiometry.
- Experiments related to the investigation of single-photon sources in terms of higher order g -function via multipoint HBT interferometer have been performed, in specific, the mode reconstruction to super resolved confocal microscopy of SPS were carried out. Experiments will be used in other NMIs and research institutes for the analysis of single-photon sources.
- A heralded single-photon source at telecom wavelengths (1.3 μm , 1.55 μm) based on SPDC photon was setup. It revealed very high photon pair rates up to 10^7 s^{-1} ($\sim 60\,000$ coincidences per sec and μW), high signal-to-background ratios of $\sim 600 \mu\text{W}^{-1}$ and a very high heralding efficiency up to 64 % were measured. Furthermore, first- and second-order coherence as well as photon statistics measurements have been performed. Measurements of the heralded $g^{(2)}$ -functions vs. pump power yield an extremely small $g^{(2)}(0) = 0.001$ at 20 nW pump power, only limited by detector dark counts.

The source is a highly efficient one, which might be exploited by companies for setting up compact and reliable single-photon sources in the infrared spectral range.

- For the heralded single-photon source at telecom wavelengths (1.3 μm , 1.55 μm) based on SPDC photon pairs the indistinguishability (purity) of the photons was measured in a Hong-Ou-Mandel (HOM) interference experiment. The generation of pure photons requires a pulsed pump laser together with the two Fibre-Bragg-Gratings to eliminate spectral correlations. The purity is observed from the visibility of the HOM-interference of two signal photons from consecutive pulses. In the experimental setup, the signal photons are sent to a fibre-based Mach-Zehnder interferometer with a delay of the inverse repetition rate of the pump laser. The idler photons are detected as heralds to project the signal photons into a heralded single photon state. Hence, the HOM interference appears in the 4-fold coincidence rate. The shape of the HOM interference dip was measured and the agreement with the first-order coherence function, as expected from theory, was validated. The visibility was measured as a function of the pump power and reaches high visibilities above 90% for low pump powers due to the absence of detector noise and multi-photon contributions.

The source developed shows indistinguishability and might be exploited by companies for setting up compact and reliable single-photon sources with indistinguishable photons in the infrared spectral range.

- Quantum-enhanced resolution in confocal fluorescence microscopy obtained by exploiting the non-classical photon statistics of single nitrogen-vacancy colour centres in diamond was experimentally demonstrated. This was achieved by developing a general model of super-resolution based on the direct sampling of the k^{th} -order autocorrelation function of the photoluminescence signal. This model shows that it is possible, in principle, to resolve arbitrarily close emitting single-photon emitters.

A new type of super-resolution microscopy was demonstrated, which might be used in other NMIs.

- A source of wavelength-degenerate (1584 nm), polarization-entangled states $|\Psi\rangle = |V_1H_2\rangle + e^{i\phi} |H_1V_2\rangle$ was realized. This utilizes a cavity which enhanced the pump power by an order of magnitude, and enabled bi-directional pumping of a periodically-poled KTP crystal. An interferometer is used to coherently entangle the down-converted states. Entanglement was confirmed by measurements demonstrating that: the occurrence of $|V_1H_2\rangle$ and $|H_1V_2\rangle$ photons cannot be inferred, the probability amplitude of $|\Psi\rangle$ being the sum of the probability amplitudes for $|V_1H_2\rangle$ and $|H_1V_2\rangle$ photons; the $|V_1H_2\rangle$ and $|H_1V_2\rangle$ photons are coherent; the classical limit ($S \leq 2$) of the Clauser-Horne-Shimony-Holt (CHSH) Bell inequality was violated by more than 8 standard deviations. Estimated lower limits with 84% confidence for the Singlet (Mayers-Yao) Fidelity of the entangled state ($\geq 90\%$) and the entanglement of formation (≥ 0.51) were obtained. The source has an 'open' architecture, enabling one to systematically perturb the properties of the state in order to evaluate the sensitivities when used for specific applications.

The setup will be the base for further investigation of entanglement and its use in metrology, which is a new field for NMIs.

4 Actual and potential impact

Actual and potential impact

The results achieved within the project will support the development of better and easier-to-use single-photon sources. The sub-ns pulse diode laser driving electronics with adjustable frequency for excitation of single-photon sources developed in the second objective of the project will be useful for further investigation of different types of single-photon sources, because it allows a scaling up of the photon flux by increasing the repetition rate instead of by increasing the excitation power. Antenna designs for simplification of photon collection were also developed and characterised by the project, as well as the high efficient waveguide-based single-photon source.

The absolute single-photon source realised within objective 3 of this project will be further developed and has the potential to enter the market as new standard source for detector calibration. A calibration service for Silicon Single-Photon Detectors (Si-SPAD) is planned in some of the NMI project partners, and is due to be established after the completion of an international comparison for detection efficiency determination.

The switched integrator amplifier, developed for the characterisation of single-photon sources in terms of wavelength, bandwidth, photon statistics, anti-bunching, and indistinguishability, i.e. for the direct measurement of single-photon fluxes in the fW-power regime with standard (analogue) Si-photodiodes, is already used in several NMIs. The amplifier allows the NMIs to measure small photon fluxes directly with standard (analogue) silicon photodiodes.

Dissemination of results

The results of this project have been reported in 28 peer-reviewed publications and activities have been presented in 72 talks or posters at scientific conferences. Furthermore, guidelines dealing with the calibration and the alignment of Silicon-based single-photon avalanche detectors were uploaded to the SIQUTE project website located at: www.ptb.de/emrp/siqute.html.

Potential impact

These outcomes will be beneficial for the scientific and metrology communities working in the corresponding fields of quantum metrology, quantum cryptography and quantum radiometry, i.e. for universities, NMIs, and companies. The results obtained will also inspire continuing work on the further development of single-photon sources and their characterisation. In the medium to long term the sources developed within this project will be further optimised in terms of higher stability and robustness, which will lead to a higher acceptance of these sources not only in the academic field, but also in an industrial environment. Single-photon sources will be used in a variety of fields such as quantum communication, radiometry, bio-photonics and medicine, medical diagnostics as well as sub-shot noise metrology, microscopy, spectrometry and interferometry. Single-photon sources will also become more “normal” or “standard” components, like lasers or LEDs to be used in highly technological applications like quantum communication, quantum computation and quantum imaging. The sources will be the basis for cheap, robust and reliable room temperature single-photon sources for use by academics and eventually schools, thus reducing the mystery and reservation surrounding “quantum technologies”.

5 Website address and contact details

A public website has been established: <http://www.ptb.de/emrp/siqute-home.html>.

The contact person for general questions about the project is Dr Stefan Kück, PTB (Stefan.kueck@ptb.de).

6 List of publications

1. D. Gatto Monticone, P. Traina, E. Moreva, J. Forneris, P. Olivero, I. P. Degiovanni, F. Taccetti, L. Giuntini, G. Brida, G. Amato, M. Genovese, “Native NIR-emitting single colour centers in CVD diamond”, *New Journal of Physics*, **16**, 053005 (2014)

2. E D Lopaeva, I Ruo Berchera, S Olivares, G Brida, I P Degiovanni and M Genovese, "A detailed description of the experimental realization of a quantum illumination protocol", *Physica Scripta*, **T160**, 014026 (2014)
3. C J Chunnillall, I P Degiovanni, S Kück, I Müller, and A G Sinclair, "Invited review article: Metrology of single-photon sources and detectors", *Optical Engineering*, **53**, 081910 (2014)
4. Y-J Wei, Y He, C-Y Lu, J-W Pan, C Schneider, M Kamp, S Höfling, D P S McCutcheon, and A Nazir, "Temperature-Dependent Mollow Triplet Spectra from Single Quantum Dot: Rabi Frequency Renormalization and Sideband Linewidth Insensitivity", *Physical Review Letters*, **113**, 097401 (2014)
5. Jakob Rosenkrantz de Lasson, Philip Trøst Kristensen, Jesper Mørk and Niels Gregersen, "Roundtrip matrix method for calculating the leaky resonant modes of open nanophotonic structures", *J. Opt. Soc. Am. A.*, **31**, 2142-2151 (2014)
6. D. Gatto Monticone, K. Katamadze, P. Traina, E. Moreva, J. Forneris, I. Ruo-Berchera, P. Olivero, I. P. Degiovanni, G. Brida, and M. Genovese, "Beating the diffraction Abbe limit in confocal microscopy via nonclassical photon statistics", *Physical Review Letters*, **113**, 143602 (2014)
7. X.-L. Chu, T. J. K. Brenner, X.-W. Chen, Y. Ghosh, J. A. Hollingsworth, V. Sandoghdar, S. Götzinger, "Experimental realization of an optical antenna designed for collecting 99% of photons", *Optica*, **1**, 203 (2014)
8. S. V. Polyakov, E. A. Goldschmidt, A. Migdall, S. Kück, F. Piacentini, G. Brida, I. P. Degiovanni, I. Ruo Berchera and M. Genovese, "Reconstruction of mode structure of faint light sources and its applications", *Physica Scripta*, **214**, T163 (2014)
9. D. Gatto Monticone, J. Forneris, M. Levi, A. Battiato, F. Picollo, P. Olivero, P. Traina, E. Moreva, E. Enrico, G. Brida, I. P. Degiovanni, M. Genovese, G. Amato, L. Boarino, "Single-photon emitters based on NIR colour centres in diamond coupled with solid immersion lenses", *International Journal of Quantum Information*, **12**, (2014)
10. J. Forneris, A. Battiato, D. Gatto Monticone, F. Picollo, G. Amato, L. Boarino, G. Brida, I.P. Degiovanni, E. Enrico, M. Genovese, E. Moreva, P. Traina, C. Verona, G. Verona Rinati, P. Olivero, "Electroluminescence from a diamond device with ion-beam-micromachined buried graphitic electrodes", *Nuclear Instruments and Methods in Physics Research Section B: Beam Interactions with Materials and Atoms*, **348** (2015)
11. Marco López, Helmuth Hofer and Stefan Kück, "Detection efficiency calibration of single-photon silicon avalanche photodiodes traceable using double attenuator technique", *Journal of Modern Optics*, **62**, S21–S27 (2015)
12. Y-J Wei, Y He, C-Y Lu, J-W Pan, C Schneider, M Kamp, S Höfling, D P S McCutcheon, and A Nazir, "Temperature-Dependent Mollow Triplet Spectra from Single Quantum Dot: Rabi Frequency Renormalization and Sideband Linewidth Insensitivity", *Physical Review Letters*, **113**, 097401 (2014)
13. D P S McCutcheon, S Unsleber, M Dambach, M Lermer, N Gregersen, S Höfling, J Mørk, C Schneider and M Kamp, "Two-photon interference from a quantum dot-microcavity system on- and off-resonance: Persistent pure-dephasing and suppression of time-jitter", *Physical Review B*, **91**, 075413 (2015)
14. D P S McCutcheon, N H Lindner and T Rudolph, "Error distributions on large entangled states with non-Markovian Dynamics", *Physical Review Letters*, **113**, 260503 (2014)
15. A Nysteen, P T Kristensen, D P S McCutcheon, P Kaer and J Mørk, "Scattering of two photons on a quantum emitter in a one- dimensional waveguide: exact dynamics and induced correlations", *New Journal of Physics*, **17**, 023030 (2015)
16. A. Meda, I. Ruo-Berchera, I. P. Degiovanni, G. Brida, M. L. Rastello, and M. Genovese, "Absolute calibration of a charge-coupled device camera with twin beams", *Applied Physics Letter*, **105**, 101113 (2014)
17. Marco López, Helmuth Hofer and Stefan Kück, "Guideline for the detection efficiency calibration of Si-SPAD, www.ptb.de/empr/siqute-home.html

18. Davide Cadeddu, Jean Teissier, Floris Braakman, Niels Gregersen, Petr Stepanov, Jean-Michel Gérard, Julien Claudon, Richard J. Warburton, Martino Poggio, Mathieu Munsch, "A fiber-coupled quantum-dot on a photonic tip", *Appl. Phys. Lett.*, **108**, 011112 (2016)
19. J. Claudon et al., "Highly directive and Gaussian far-field emission from "giant" photonic trumpets", *Applied Physics Letter*, *Appl. Phys. Lett.* **107**, 141106 (2015)
20. J. Forneris, P. Traina, D. Gatto Monticone, G. Amato, L. Boarino, G. Brida, I. P. Degiovanni, E. Enrico, E. Moreva, V. Grilj, N. Skukan, M. Jakšić, M. Genovese, P. Olivero, "Electrical stimulation of non-classical photon emission from diamond color centers by means of sub-superficial graphitic electrodes", *Sci. Rep.*, **5**, 15901 (2015)
21. F. Piacentini, M. P. Levi, A. Avella, M. López, S. Kück, S. V. Polyakov, I. P. Degiovanni, G. Brida, M. Genovese, "Positive operator-valued measure reconstruction of a beam-splitter tree-based photon-number-resolving detector", *Optics Letters*, **10.1364/OL.40.001548**
22. J. Forneris, A. Tengattini, S. Ditalia Tchernij, F. Picollo, A. Battiato, P. Traina, I.P. Degiovanni, E. Moreva, G. Brida, V. Grilj, N. Skukan, M. Jakšić, M. Genovese, P. Olivero, "Creation and characterization of He-related color centers in diamond", *Journal of Luminescence*, <http://dx.doi.org/10.1016/j.jlumin.2016.06.039>
23. K. Dhoska, H. Hofer, M. Lopez, T. Kübarsepp, S. Kück, "Alignment position method for SPAD detector calibration and homogeneity", *Intl J. Of Sci Reports*, **1**, 271-274 (2015)
24. G. Porrovecchio, M. Šmid, M. López, H. Hofer, B. Rodiek, S. Kück, "Comparison down to sub-100-fW optical power level between a high sensitive, low noise Silicon photodiode and a low optical flux measurement facility based on a double attenuator technique, *Metrologia*, **53**, 1115–1122 (2016)
25. Beatrice Rodiek, Marco López, Helmuth Hofer, Xiao-Liu Chu, Stephan Götzinger, Stefan Kück, "Characterisation of nitrogen-vacancy based single-photon sources", *DGaO-Proceedings*, http://www.dgao-proceedings.de/download/117/117_p32.pdf
26. M. López, G. Porrovecchio, H. Hofer, B. Rodiek, M. Smid, S. Kück, "Calibration of Si-SPAD detectors using the double attenuator technique and a low noise silicon photodiode", *DGaO-Proceedings*, http://www.dgao-proceedings.de/download/117/117_p28.pdf
27. B. Rodiek, M. López, H. Hofer, G. Porrovecchio, M. Šmid, X.-L. Chu, S. Götzinger, V. Sandoghdar, S. Lindner, C. Becher, S. Kück, "Experimental realization of an absolute single-photon source based on a single nitrogen vacancy center in a nanodiamond", *Optica* **4**, 71 (2017)
28. Aigar Vaigu, Geiland Porrovecchio, Xiao-Liu Chu, Sarah Lindner, Marek Smid, Albert Manninen, Christoph Becher, Vahid Sandoghda, Stephan Götzinger, Erkki Ikonen, "Experimental demonstration of a predictable single photon source with variable photon flux", <https://doi.org/10.1088/1681-7575/aa5ba2> *Metrologia* **54**, 218-223 (2017)
29. M. Bock, A. Lenhard, C. Chunnillall, and C. Becher, "A highly efficient heralded single photon source for telecom wavelengths based on a PPLN waveguide", *Opt. Express* **24**, 23992 (2016)
30. N. Gregersen, D. P. S. McCutcheon, J. Mørk, J.-M. Gérard, and J. Claudon, "A broadband tapered nanocavity for efficient nonclassical light emission," *Opt. Express* **24**, 20904–20924 (2016)
31. X.-L. Chu, S. Götzinger, V. Sandoghdar, A single molecule as a high-fidelity photon gun for producing intensity-squeezed light, *Nature Photonics* **11**, 58–62 (2017), doi:10.1038/nphoton.2016.236